

## **Diffusion, atomic transport, and ordering in Al-Zr alloys: FCC and liquid phases.**

Yuri Osetsky\*, Alex Plotkowski, and Ying Yang

<sup>1</sup>Materials Science and Technology Division, Oak Ridge National Laboratory. Oak Ridge, TN 37831, USA.

Additive manufacturing of materials with controlled microstructure demands knowledge of atomic scale properties near the solid-liquid transition state. Many of these properties are not affordable by experimental techniques and computer modeling is the possible solution to the problem. In this paper, we present the results of an extended atomistic study of intrinsic atomic transport due to vacancy diffusion in FCC and L12 solid phases and diffusion in the liquid phase of Al-Zr alloys. A deceleration of the overall self-diffusion was observed when Zr was added to Al. The effect was stronger in the solid and weaker in the liquid. Additionally, the effect was strongly temperature dependent in the solid phases, but not in the liquid. Atomic transport was chemically biased: transport of Zr atoms was significantly slower than that of Al atoms, and this bias effect was stronger in the solid phases. The overall diffusion and chemical ordering processes in the liquid state were five to six orders in magnitude faster than in the solid. Chemical short-range order parameters in the liquid saturated at values close to those in the ordered L12 structure of Al<sub>3</sub>Zr. Chemical and structural ordering in the solid phases was negligible over the modeled microsecond time scale. The results are discussed in view of optimizing additive manufacturing parameters for the controlled formation of metastable L1<sub>2</sub> precipitates.

- Corresponding author e-mail: [osetskiyyn@ornl.gov](mailto:osetskiyyn@ornl.gov)

*This manuscript has been co-authored by UT-Battelle, LLC under Contract No. DE-AC05-00OR22725 with the U.S. Department of Energy. The United States Government retains and the publisher, by accepting the article for publication, acknowledges that the United States Government retains a non-exclusive, paid-up, irrevocable, worldwide license to publish or reproduce the published form of this manuscript, or allow others to do so, for United States Government purposes. The Department of Energy will provide public access to these results of federally sponsored research in accordance with the DOE Public Access Plan.*

## 1. Introduction

Ni-based superalloys have an exceptional combination of high temperature mechanical properties due to the formation of a high volume-fraction of coherent  $L1_2$ -type  $Ni_3Al$  precipitates in the FCC (Face Centered Cubic) matrix [1]. Despite the presence of similar  $L1_2$  phases in many aluminum alloy systems, the formation of such microstructures in light-weight Al based alloys remains a challenge. While some Al-M systems such as Al-Sc and Al-Er alloys can form  $L1_2$ -type precipitates within the FCC crystal lattice [2], most other  $Al_3M$  compounds do not have thermodynamically stable  $L1_2$  phase. Additionally, because of the characteristically low solubility of many  $Al_3M$  forming elements in Al, even Al-Sc and Al-Er alloys do not produce the high volume-fractions of precipitates that lead to improved performance in Ni-based alloys.

A promising method for increasing the volume fraction of dispersive tri-aluminide precipitates is therefore to increase the amount of the solute content in the Al FCC solid solution through non-equilibrium solidification. Such an effect is well known from the research of rapid solidification processes [3,4], during laser melting [5] and melt spinning [6]. Recent advances in additive manufacturing (AM) suggest an approach for achieving high solidification rates in the bulk structures, motivating a renewed focus on the development of high-performance aluminum alloys [5], including those with strengthening  $L1_2$  precipitates [8-10]. High solidification rates are effective for extending solubility because solute partitioning between liquid and solid varies with increasing cooling rates. Most conventional casting methods operate in a regime between the lever-rule and Scheil solidification modes where the liquid-solid interface compositions follow the equilibrium liquidus and solidus lines [11]. With increasing solidification rates, the interface departs from local equilibrium and follows non-equilibrium solidus and liquidus lines. Complete solute trapping occurs when the liquidus and solidus lines converge [12]. The degree of solute trapping depends on competition between solute diffusion in the liquid and the solid/liquid interface growth velocity. The resulting supersaturated solutions have a large driving force for precipitation upon subsequent aging, which also depends on thermodynamic and kinetic considerations such as solubility and diffusivity of the solute in the solid solution. As a result, it is of great interest to qualify the diffusion mechanisms and quantify their parameters for  $Al_3M$  forming solutes in both the liquid and solid phases at elevated temperatures.

Zr is a common element added to Al alloys to form  $\text{Al}_3\text{Zr}$  which presents advantages via two mechanisms. First, primary  $\text{Al}_3\text{Zr}$  particles form from the liquid and act as potent nucleation inoculants for FCC Al, resulting in the formation of refined equiaxed grains and reducing the susceptibility to the formation of solidification cracks. Second, Zr in solution within the FCC aluminum matrix can form dispersive nano-scale  $\text{L1}_2$  particles [13,14] during a post-process heat treatment, which promotes precipitation strengthening for enhanced mechanical properties. While the equilibrium structure of  $\text{Al}_3\text{Zr}$  is tetragonal ( $\text{DO}_{23}$ ), diffusional decomposition [15, 16, 17] of supersaturated Al–Zr solid solutions occurs initially by the formation of metastable nanometer-scale  $\text{Al}_3\text{Zr}$  precipitates with the cubic  $\text{L1}_2$  structure [13, 14].  $\text{Al}_3\text{Zr}$   $\text{L1}_2$  precipitates are coherent, structurally stable, and provide hardening even after long times of heat treatment (400 h) at  $\sim 700$  K.  $\text{Al}_3\text{Zr}$  precipitates present a series of different morphologies and structures depending on processing conditions, including spheroidal, rod-like, petal-like, cauliflower, cellular, and disk-like (see [18] and references there). Formation of  $\text{L1}_2$   $\text{Al}_3\text{Zr}$  precipitates in rapidly solidified alloys with 5-15 at.% Zr and the subsequent transformation towards  $\text{DO}_{23}$  precipitates during annealing at the temperature range 573-773K was observed in [19]. The solubility limit of Zr in Al is low in both solid ( $\sim 0.08$  at.%) and liquid ( $\sim 0.03$  at.%) phases and weakly increases at higher temperatures [17, 20]. Recent studies on Zr in Al-Cu-Ce and Al-Ni-Ce alloys show beneficial role in improving strength through precipitation hardening [10]. Greater strengthening is anticipated if the concentration of Zr in the FCC solid solution is increased beyond the thermodynamic equilibrium conditions using additive manufacturing. Significantly increasing the supersaturation of Zr in the Al FCC structure requires an accurate understanding of Zr diffusion in solid FCC and liquid phases and its relationship to the velocity of the liquid/solid interface and local thermal gradient.

Unfortunately, the information on diffusion mechanisms and diffusion parameters in the Al-Zr system is very limited. The literature reports mainly observations of precipitation in annealing experiments [15, 16] and thermodynamic treatment of CALPHAD [21] or kinetic Monte Carlo models with some rough assumptions on the diffusion mechanisms sometimes based on *ab initio* obtained defect energetics [22, 23]. Recent theoretical, atomistic, and mesoscale simulations have demonstrated that the defect diffusion and atomic transport in alloys can be characterized by strong correlations and specific effects associated with the so-called chemically biased diffusion [24,25]. Important factors include temperature-related fluctuations of the potential, kinetic and free energy, atomic vibrations and their dependence on the local microstructure and composition,

dynamic changes in the local free energy landscape, etc. All these depend on the ambient temperature, defect nature, distribution of constitutive elements and/or microstructural features. Due to rapid thermal cycles characteristic of additive manufacturing, non-equilibrium microstructures are frequently observed. Thus, phase transformations, chemical and structural ordering, segregation and precipitation follow non-equilibrium mechanisms for which parameters are difficult to measure experimentally. Atomistic modeling provides the ability to decouple defect formation and dynamics and study them separately under controlled conditions. Diffusion in chemically complex alloys is an example where atomistic modeling may clarify the governing mechanisms (see e.g. [24, 25]). No detailed atomistic study of diffusion in the solid or liquid phases of the Al-Zr system was found in literature and the present article aims to fill up this gap. We describe here the results of an extensive atomistic study of diffusion in solid and liquid phases of pure Al and some Al-Zr alloys. The main aim is to understand diffusion and atomic transport mechanisms, alloy ordering processes, and obtain diffusion parameters in Al-Zr systems. This information is necessary for understanding and predicting higher-level processes during additive manufacturing of alloys with controlled microstructures.

## **2. Modeling approaches, interatomic potentials, and results treatment.**

Molecular dynamics (MD) modeling is the most accurate technique to study thermally activated diffusion in materials. Two main parameters affect the accuracy of MD for studying diffusion: interatomic potentials (IAPs) and modeling time. IAPs [26, 27] used here were thoroughly tested and the results on defect properties and thermal expansion presented below allow us to conclude that the IAPs used here [27] are qualitatively and in many cases quantitatively accurate in describing properties of Al-Zr system relevant to the current study. Accurate estimation of diffusion coefficients demands long-time modeling to provide sufficiently long defect/atom trajectories for accurate diffusion approximations. The method applied for estimating the proper modeling time to ensure accurate calculations is described here.

### ***2.1 Interatomic potentials: properties and testing.***

The potentials used in this study [27] were fitted to the basic properties of the pure elements and some binary compositions such as lattice parameters, cohesive energies, bulk

modulus, and elastic moduli. Some additional properties relevant to diffusion in the Al-Zr system were tested here via directed modeling using these IAPs and density-functional theory (DFT) [28]. For DFT modeling we used the generalized gradient approximation (GGA) and the Perdew-Burke-Ernzerhof [29] parametrization of the electronic exchange-correlation functional. The energy of pure Al and Al-Zr mixtures for perfect and defected crystals were calculated using the plane-wave basis projector augmented-wave approach [30] as implemented in the Vienna Ab-initio Simulation Package (VASP) [31]. A plane-wave energy cutoff of 350 eV and  $2 \times 2 \times 2$  k-mesh were used to obtain defects formation energy in  $4 \times 4 \times 4$  supercell containing 256 lattice sites. Initially in the perfect system, the shape, volume, and atomic positions were relaxed until the total pressure dropped below 0.1 kBar and forces acting on atoms did not exceed  $10^{-5}$  eV/Å. Defects, *e.g.*, vacancies, Zr substitution, and their combinations, were then modeled by inserting in the above perfect crystal and optimizing only atomic positions with the same accuracy. Properties obtained with this approach are presented in Table 1 together with the available experimental data.

The IAPs were found to accurately describe the properties of pure Al, except of the vacancy formation energy, which is overestimated by the IAP: 0.94eV versus 0.65 from VASP calculations and 0.67-0.72 measured in experiments [32-36]. There are no experimental data for properties of Zr solute in Al, so we can compare these IAPs only with our VASP modeling. The energies calculated by DFT and with IAPs [27] are presented in Table A1 and are in good agreement with a few exceptions. Thus, the binding energy of Zr substitution with Al vacancies in the nearest neighbor site,  $E_{V-Zr_1}^b$ , is almost zero with IAPs (0.004eV), but is strongly negative with VASP (-0.352eV). The binding energy with a vacancy in the second neighbor site,  $E_{V-Zr_2}^b$ , are positive in both approaches although it is lower with IAPs than with VASP *i.e.*, 0.061eV vs 0.195eV. Zr substitution dimer interaction energies in the Al matrix are very close for both IAPs and VASP calculations.

Cohesive energy per atom,  $E_{Coh}^{Al_3Zr}$ , for  $Al_3Zr$  compounds was according to :  $E_{Coh}^{Al_3Zr} = (3 E_{atom}^{Al} + E_{atom}^{Zr} - E_{molecule}^{Al_3Zr})/4$ , where  $E_{atom}^{Al}$  and  $E_{atom}^{Zr}$  are cohesive energy in perfect fcc Al and hcp Zr, and  $E_{molecule}^{Al_3Zr}$  is the energy of perfect  $Al_3Zr$  molecule in  $DO_{23}$  or  $L1_2$  structures. The cohesive energy for the intermetallic  $Al_3Zr$  reproduced by the IAPs are somehow above the data obtained by VASP modeling and experimental study as seen in Table A1. The difference in  $E_{Coh}^{Al_3Zr}$

for DO<sub>23</sub> or L1<sub>2</sub> phases is also slightly overestimated with IAPs compared to VASP results: 0.014eV/atom vs 0.002eV/atom. This mean that the corresponding phase transformations should be somehow enhanced in modeling with these IAPs. However, it is unlikely may have any effect at the time-scale of MD modeling approach.

**Table 1.** Properties of some Al-Zr compounds and defects.

		IAP	DFT	Exp.
<b>Al</b>				
$E_{coh}$		3.392	3.747	3.386 [32]
$a_0$		4.050	4.050	4.049 [32]
$E_{vac}^f$		0.941	0.654	0.67-0.77 [33-36]
<b>Zr in Al</b>				
$E_{Al-Zr}^{substitution}$		-5.014	-5.889	
$E_{V-Zr_1}^b$		0.004	-0.352	
$E_{V-Zr_2}^b$		0.046	0.195	
$E_{2Zr_1}^b$		-0.308	-0.200	
$E_{2Zr_2}^b$		0.084	0.116	
<b>Al<sub>3</sub>Zr</b>				
$E_{coh}$	DO <sub>23</sub>	-0.571 eV/atom	-0.509 eV/atom [37] -0.489 eV/atom	5.241 [42]
	L1 <sub>2</sub>	-0.557 eV/atom	-0.464 eV/atom [37] -0.462 eV/atom	
$a_0$	DO <sub>23</sub>	3.996	4.009 [37] 4.021	4.001 at 12K 4.008 at 300K [44] 4.007 [45]
	L1 <sub>2</sub>	4.065	4.110	

Intermetallic Al<sub>3</sub>Zr in the DO<sub>23</sub> phase was found to be slightly more stable than in the L1<sub>2</sub> with the difference in cohesive energy 0.025eV whereas in DFT calculations resulted in smaller

difference in cohesive energy  $0.009\text{eV}$ . Note, that earlier results [37] reported the cohesive energy difference between  $\text{DO}_{23}$  and  $\text{L1}_2$  to be equal to  $0.028\text{ eV}$ . We assume that this energy difference is too negligible to distinguish phase stability difference in MD modeling and produce qualitative difference in of defects diffusion and alloy ordering.

The subject of the present study is thermally-activated diffusion and atomic ordering in solid and liquid phases. A direct and accurate technique to study the atomic transport via thermally-activated processes is molecular dynamics (MD) (see [25, 38]). The MD approach for studying diffusion has clear advantages, such as: a) the possibility to follow, and trace any atom, group of atoms, or components, b) the complete monitoring of the defect motion, c) the ability to consider a wide range of compositions, microstructures, and external variable parameters temperature, stresses, etc., and d) self-consistent consideration of vibrational and chemical potential effects. The most accurate approach is the *ab initio* MD that, however, demands large computational resources and so far, has been applied only to interstitial atom mechanisms in solids and some liquid systems in small,  $\sim 100$  atoms, systems [24, 39, 40]. The usage of empirical IAPs allows classical MD to extend diffusion studies to  $\mu\text{s}$  time- and a few nm spatial- scales. These scales are important for modeling alloys and provide high statistics of defect jumps, when the defect visits a large number of non-equivalent configurations, and, thus, high accuracy in estimating diffusion parameters, *e.g.*, diffusion coefficients, as well as diffusion and ordering mechanisms. We applied the MD by modeling the constant-temperature, constant-pressure (NPT) ensembles at different temperatures in crystalline and liquid phases. All modeled systems were cubes with size  $10a$ , where  $a$  is the composition and temperature dependent lattice parameter that provides zero pressure in the modeled crystal. The system contained 4000 lattice sites, and 3999 and 4000 mobile atoms when modeling vacancy and liquid phase diffusion, respectively. Periodic boundary conditions were applied in all directions. The crystal size provided accurate modeling even for the lowest alloy concentration used here, that is 2at.% Zr, corresponds to only 80 impurity atoms. Due to a very large difference in atomic masses Al and Zr, *i.e.*, 27 and 92 correspondingly, MD modeling is very sensitive to the value of the time step,  $t_0$ , used for integration of the motion equation via the velocity Verlet algorithm. Depending on the temperature we used  $t_0 = 0.5 - 1.0$  femtoseconds (*fs*) for modeling solid state and  $t_0 = 0.0025 - 0.025$  *fs* for modeling the liquid state.

Using this approach, we performed a preliminary study to ensure that the IAPs accurately reproduce thermodynamic properties such as thermal expansion. For this, we modeled equilibrium states of perfect FCC, L1<sub>2</sub> and liquid phase of pure Al and Al<sub>3</sub>Zr systems at different temperatures. The results of the temperature dependence of equilibrium atomic volume are presented in Fig.1, and compared with the corresponding treatment of the available experimental data. Experimental data for liquid Al were derived from the temperature dependence of density obtained in [40], data for FCC Al were derived from the lattice expansion results reported in [41]. Comparison in Fig.1 demonstrates a good agreement between modeled and experimental data for both quantitative data and the coefficient of thermal expansion, derived as  $\alpha = \frac{1}{V} \left( \frac{\partial V}{\partial T} \right)_P$ . Thus, IAPs reproduce  $\alpha$  equal to  $7.72 \times 10^{-5} \text{ K}^{-1}$  and  $9.45 \times 10^{-5} \text{ K}^{-1}$  for the FCC and liquid Al, respectively. The corresponding treatment of experimental data results in slightly higher values of  $\alpha$ , e.g.,  $8.09 \times 10^{-5} \text{ K}^{-1}$  for FCC and  $11.0 \times 10^{-5} \text{ K}^{-1}$  for liquid Al. For the Al<sub>3</sub>Zr L1<sub>2</sub> phase, the value of  $\alpha$  were estimated by linear interpolation of temperature dependent equilibrium volume modeled with IAPs results in  $4.2 \times 10^{-5} \text{ K}^{-1}$ . We did not find experimental data for the thermal expansion of the Al<sub>3</sub>Zr intermetallic. In estimating the thermal expansion in ZrB<sub>2</sub>/Al<sub>3</sub>Zr/AA5052 composites in [42] the value  $1.25 \times 10^{-5} \text{ K}^{-1}$  was used; however, the source was unclear. The DFT modeling of thermal expansion in [42, 43] reported that the thermal behavior of  $\alpha_{Al_3Zr}$  in both L1<sub>2</sub> and DO<sub>23</sub> is very similar. At 300K the value  $3.87 \times 10^{-5} \text{ K}^{-1}$  was reported in [42] and  $\alpha_{Al_3Zr} \sim 3.9 \times 10^{-5} \text{ K}^{-1}$  in [43] for the L1<sub>2</sub> phase. These values are very close to  $\alpha_{Al_3Zr} = 4.2 \times 10^{-5} \text{ K}^{-1}$  estimated here for the L1<sub>2</sub>.

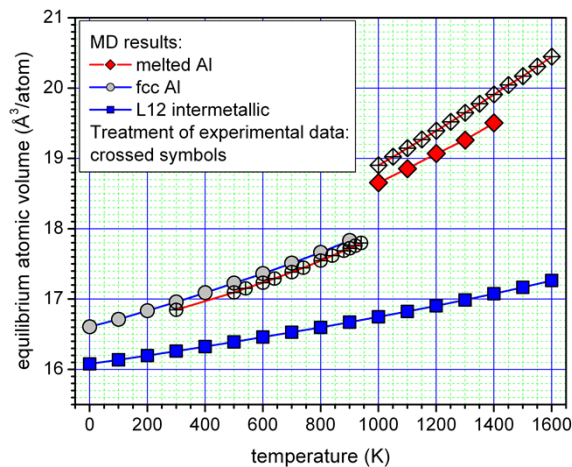


**Fig.1** Equilibrium volume as function of temperature for melted (diamonds) and FCC (circle) pure aluminium and L12 phase of the Al<sub>3</sub>Zr alloy (square). Solid symbols are modeling results, crossed symbols are treatment of published experimental data [40, 41].

The results on defect properties and thermal expansion presented in Sections 2.1-2.2 allow us to conclude that the IAPs used here [26, 27] are qualitatively and in many cases quantitatively accurate in describing properties of Al-Zr system relevant to the current study. We would like to mention that the IAPs energy parameters published in [26, 27] lost the conversion coefficient from joules to electronvolts. To fix this, the coefficients presented in ref. [27] (Table 1) were corrected:  $A_1$  and  $A_{1m}$  divided by 1.6022, and coefficients  $A_2$  and  $A_{2m}$  divided by 1.6022<sup>2</sup>.

## ***2.2 Research approaches and treatment techniques.***

In this research, we studied the diffusion and atomic transport in the solid and liquid phases of pure Al and Al-based alloys with 2, 5 and 25 at.% Zr, which further will be denoted as Al-2Zr, Al-5Zr and Al-25Zr alloys, respectively. The main parameter characterizing the atomic diffusion process is the tracer diffusion coefficient,  $D$ , that in MD modeling can be obtained with sufficient precision using the Einstein equation:

$$D = \frac{\langle R^2 \rangle}{2nt}. \quad (1)$$

Here  $\langle R^2 \rangle$  is the mean atomic square displacement of tracer atoms over time  $t$ ,  $n$  is the dimensionality of atomic jumps ( $n=3$  for the three-dimensional diffusion). The average is performed over the ensemble of  $M$  tracer atoms, each displaced by a vector  $r_i$ :  $\langle R^2 \rangle = \sum_{i=1}^M r_i^2 / M$ .

Liquid phase diffusion can be simulated correctly in systems of typical size for MD studies (a few hundred to few thousand atoms) without considering defects and/or particular diffusion mechanisms. In this case eq.(1) directly results in the value of tracer diffusion coefficient per atom.

In contrast, solid state diffusion occurs due to thermally-activated vacancy hops, where the thermally-equilibrium concentration  $c_v$ , is very low,  $\sim 10^{-4}$ , near the melting temperature, and exponentially decreases at lower temperatures. In practice, it is common to introduce a vacancy into the simulation domain to create a vacancy concentration equal to  $N^{-1}$  ( $N$  is the total number of atoms in the system). In this case, eq. (1) results in the value of tracer diffusion coefficient related to the modelled vacancy concentration that is  $N^{-1}D$ , therefore, to obtain the value of tracer  $D$  eq. (1) should be multiplied by  $N$ .

In eq. (1), the average of atomic square displacements is either over all atoms in the system (all atoms are tracers:  $M=N$ ) to obtain the total tracer diffusion coefficient or over the specific

species to obtain the partial tracer diffusion coefficient. Thus, the component A diffusion coefficient in the alloy is estimated as:

$$D_A = N \frac{\sum_{i=1}^{N_A} r_i^2}{6tN_A} = \frac{1}{c_A} \frac{\sum_{i=1}^{N_A} r_i^2}{6t}, \quad (2)$$

here we used the definition of the component A concentration:  $c_A = N_A/N$ , where  $N_A$  is the number of A-type atoms in the modelled system. For the Al-Zr binary system, the total tracer diffusion coefficient can be represented as a sum of partial diffusivities weighted with the corresponding atomic fractions:

$$D = D_{Al}c_{Al} + D_{Zr}c_{Zr}. \quad (3)$$

Other diffusion characteristics, such as the defect jump frequency, the correlation factor of defect jumps and the defect diffusion coefficients, can be estimated using different approaches (see, *e.g.* [44]), which are applicable here only for the low temperature solid phases.

Using the  $D$  values for different temperatures, one can represent the total and partial diffusivities in the form of the Arrhenius relationship with the corresponding pre-exponential factor,  $D^0$ , and effective activation energy of the modelled process,  $E^a$ :

$$D = D^0 \exp\left(-\frac{E^a}{k_B T}\right), \quad (4)$$

where  $k_B$  is the Boltzmann constant and  $T$  is the absolute temperature. Here we model only atom migration, but no defect formation, and thus the activation energy is, in fact, an effective migration energy of the modelled diffusion mechanism.

In estimating self-diffusion coefficient at equilibrium conditions, one should estimate a temperature dependent vacancy concentration. In this paper we use the vacancy formation energy,  $E^f = 0.941$  eV (see Table 2) in pure Al obtained with IAPs [27], and the mono-vacancy formation entropy  $\sim k_B$  (see, *e.g.* [46]). In this approach, the vacancy concentrations in Al is  $c_v \approx 3 \exp\left(-\frac{E^f}{k_B T}\right)$ , and the solid state self-diffusion coefficient is

$$D^{SD} \approx 3D^0 \exp\left(-\frac{E^f + E^a}{k_B T}\right). \quad (5)$$

There are a few uncertainties when comparing the MD results with experiments, the most significant being the estimation of the thermally-equilibrium vacancy concentration. First, the value of  $E_{vac}^f$  is overestimated with the IAPs used (see Table 2). Second, since we modelled here a single vacancy, the pre-exponential factor should correspond to the mono-vacancy. Although the mono-vacancy is the most probable defect in the system, the possibility of di-vacancy formation

was reported in [46], involving more than two-fold higher formation entropy. Correspondingly, some experimental studies reported deviations of the diffusion coefficient from the Arrhenius law, possibly due to vacancy double jumps [46] and/or di-vacancy diffusion at high temperatures [47, 48]. While these complications could introduce uncertainty in the solid-state diffusion parameters, the MD diffusivity estimation from eq. (1) is reasonable and can be directly used in the liquid state. In the present article comparison with the measurements are made only for pure Al in the solid and liquid phases.

Modeling time is an important parameter in MD study of diffusion. In pure metals, a few tens of ns may be enough, whereas in alloys microseconds time may be too short. Examples of the temporal evolution of ASDs due to vacancy migration in solid and diffusion in liquid phases of the Al-5Zr alloy are presented in Fig.2. The most complicated cases are associated with the lowest temperature, i.e.  $T=400\text{K}$  for FCC and  $800\text{K}$  for liquid Al-5Zr alloy. Fig.3 demonstrates how the diffusion coefficients converge with the modeling time. It can be seen, vacancy diffusion at  $400\text{K}$  demands quite a long modeling time, above a microsecond, whereas diffusion in liquid converges quite rapidly, just after  $0.3\text{-}0.4\text{ ns}$ . With the increasing temperature, the convergency improves significantly.

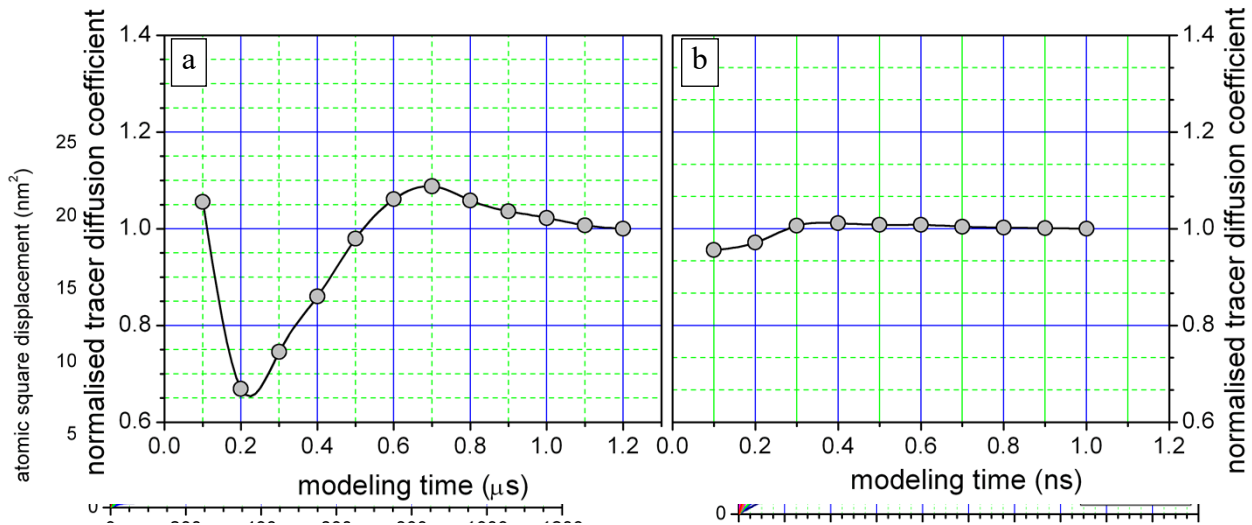


**Fig.3** Convergence of the tracer diffusion coefficient for (a) vacancy migration ( $T=400\text{K}$ ) in FCC phase and (b) diffusion ( $T=800\text{K}$ ) in melted Al5Zr alloy as function of MD modeling time. Diffusion coefficients are normalized per the corresponding value for the longest modeling time in each case, e.g.  $D^*=5.16 \times 10^{-11} \text{m}^2/\text{s}$  in FCC and  $D^*=1.78 \times 10^{-9} \text{m}^2/\text{s}$  in liquid phases.

### 2.3 Monitoring ordering process.

During modeling, evolution of chemical ordering of initially random alloys was monitored by on-the-fly calculation of the chemical short-range order (CSRO) parameter,  $\alpha_{ij}^k$ , using the Warren-Cowley definition [49]:

$$\alpha_{ij}^k = 1 - \frac{p_{ij}^k}{c_i}. \quad (6)$$

Here,  $p_{ij}^k$  is the conditional probability of finding an  $i$  atom around the  $j$  atom in its  $k$ th nearest-neighbor shell, and  $c_i$  is the overall concentration of  $i$  atoms. In random alloys,  $\alpha_{ij}^k = 0$ , since the probability of finding  $i$  and  $j$  atoms corresponds to their concentrations. The case  $\alpha_{ij}^k < 0$  suggests that  $i$ - $j$  bonds are dominantly present in the system, and when  $\alpha_{ij}^k > 0$ ,  $i$ - $j$  bonds are less probable. Initially created alloys are fully random with all  $\alpha_{ij}^k \approx 0$ . During diffusion, a certain CSRO develops, and its level determines the ordering of the corresponding species. Here we were interested mainly in  $\alpha_{ZrZr}^k$  related to ordering of Zr atoms. We calculated this through the first three coordination spheres, *i.e.*, for  $k=1-3$ . We also note that we used the modified CSRO parameter for presentation:  $\alpha^* = -\alpha_{ij}^k$ , which simplifies understanding of the plots: positive values mean ordering, whereas negative values mean repulsion of the corresponding species. Note that the CSRO parameter characterizes only the chemical but not the structural order.

## 3. Results

### 3.1. pure Al

The temperature dependence of the tracer diffusion coefficient in pure Al calculated via eq. (1) is presented in Fig.4 together with experimental results reported in [47, 48, 50-55]. Modeling results are systematically lower than experimental. The discrepancy is first related to the overestimated vacancy formation energy calculated with IAPs that results in an underestimated vacancy concentration. However, experimental results have also demonstrated a significant scattering in diffusivity and its parameters such as the pre-exponential factor,  $D_0$ , and the self-diffusion activation energy, usually taken as  $E_{SD} = E_{vac}^f + E^a$ . Modeling vacancy diffusion results in  $D_0 = 0.45 \times 10^{-5} \text{m}^2/\text{s}$  and  $E_{SD}^a = 1.29 \text{ eV}$ , whereas experimental data vary as  $D_0 = 1.0 \times 10^{-5} \text{m}^2/\text{s}$ ,  $17.1 \times 10^{-5} \text{m}^2/\text{s}$ ,  $4.5 \times 10^{-5} \text{m}^2/\text{s}$ , and  $E_{SD}^a = 1.32 \text{ eV}$ ,  $1.47 \text{ eV}$ ,  $1.43 \text{ eV}$  reported in [54, 50, 55] respectively. One can see that while the self-diffusion activation energy varies weakly, the pre-

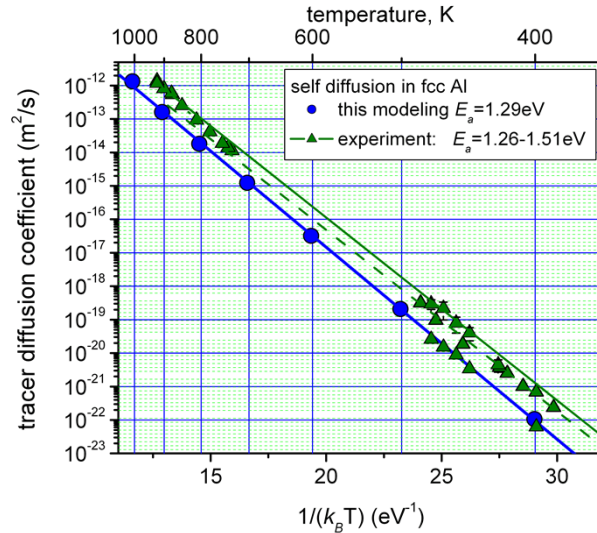


**Fig.4** Tracer diffusion coefficient obtained in modeling vacancy migration in pure FCC Al (blue line and circles) and experimental results (green line and triangles) obtained by different techniques such as tracer diffusion [48], annealing of vacancies [50], voids [51], and dislocation loops in quenched Al [52], NMR measurements [47, 48, 53, 54] and their combinations.

exponential factor values vary by more than an order of magnitude. Thus, the uncertainty in the value of  $D_0$  for the modeled case, associated with the uncertainty in vacancy formation entropy, is accompanied with corresponding uncertainty in the experimental data. The only conclusion can be made on the value of the self-diffusion activation energy and  $E_{SD} = 1.29 \text{ eV}$  obtained in modeling is within the range  $1.26\text{-}1.51 \text{ eV}$  reported in different experiments. An Arrhenius treatment of diffusion coefficients obtained directly from eq. (1) resulted in the effective vacancy migration

energy  $E^a=0.38$  eV (see Table 1). This value is lower than that estimated from experiments for vacancy migration energy e.g. 0.49 eV [51], 0.63 eV [47], and 0.61 eV [56].

The results of modeling diffusion in the liquid phase are shown in Fig.5 together with the available experimental and modeling data. The present modeling results can be described by the following Arrhenius parameters:  $D_0 = 8.2 \times 10^{-8} \text{m}^2/\text{s}$  and  $E^a=0.23$  eV. An Arrhenius treatment of the experimentally obtained data results in  $D_0 = 8.6 \times 10^{-8} \text{m}^2/\text{s}$  and  $E^a=0.21$  eV [57] and  $E^a=0.28$  eV [58]. DFT MD modeling in [59] can be described with the following parameters  $D_0 = 7.6 \times 10^{-8} \text{m}^2/\text{s}$  and  $E^a=0.22$  eV. The results obtained in classical MD modeling with the two “best” EAM potentials in [60] can be parameterized with  $D_0 = (13.3-18.8) \times 10^{-8} \text{m}^2/\text{s}$  and  $E^a=0.26-0.31$  eV. Our

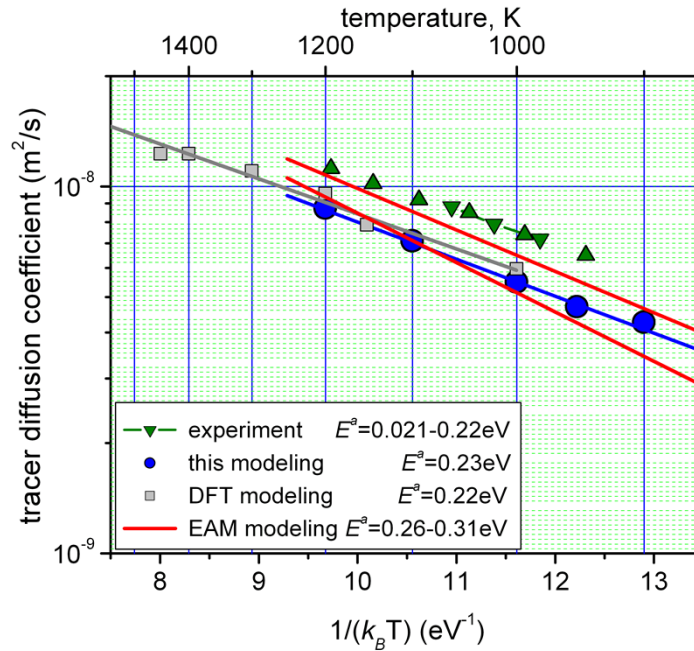


**Fig.5** Self diffusion coefficient obtained in modeling diffusion in melted pure Al (blue line and circles). Experimental results obtained in [57, 58] are shown by green symbols, *ab initio* modeling results [59] are shown by gray squares, and some results of classical modeling from [60] are shown by red lines.

results are close to those obtained in DFT modeling and both are about 40% lower than the experimental data whereas the effective activation energy  $E^a$  is practically the same for these three cases. Other classical modeling results [60, 61] mostly overlap with our results, although they have higher activation energies, from 0.26eV to 0.31eV. Unlike vacancy diffusion in FCC Al, in the liquid phase there is no uncertainty related to vacancy formation discussed above and the results obtained here are more reliable than those in FCC phase.

Fig.6 shows diffusion coefficients obtained here in the liquid and solid FCC Al compared to experimental data. Our primary interest is in the temperatures near melting. For the IAPs used here for Al the solid/liquid coexistence temperature was estimated as  $T_{s/l} \cong 950\text{K}$  which is very close to the experimentally obtained melting temperature,  $T_m \cong 934\text{K}$  and near this temperature diffusivity in the liquid is about five orders in magnitude faster than in the FCC phase.

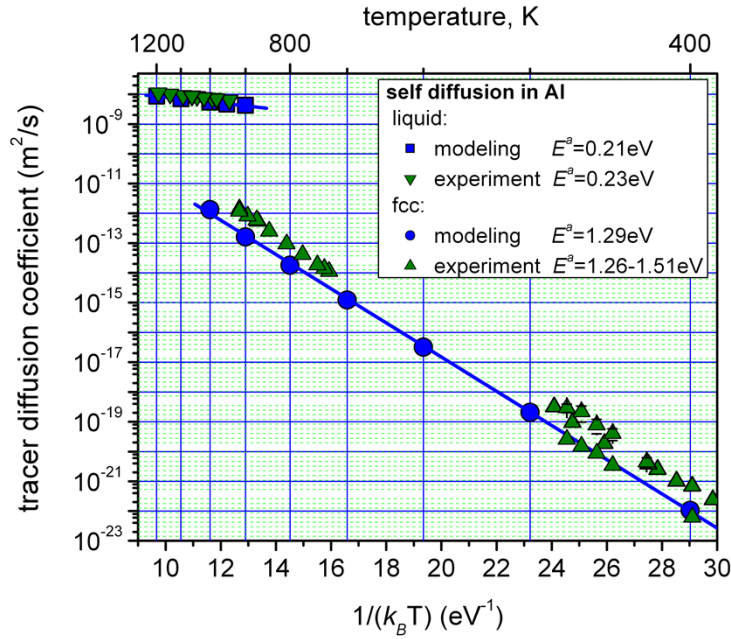


**Fig.6** Self diffusion coefficient obtained in modeling diffusion in melted and FCC solid pure Al (blue symbols and lines) and some experimental results (green triangles).

### 3.2. Low Zr alloys

The total tracer diffusion coefficients in FCC pure Al, Al-2Zr and Al-5Zr alloys are

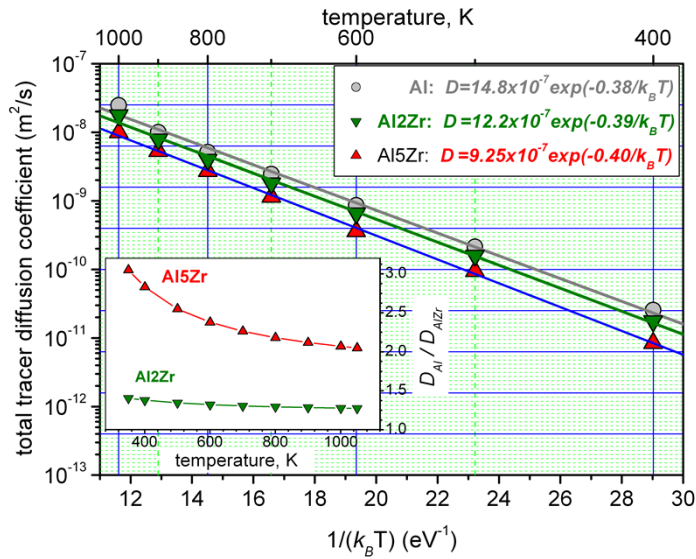


**Fig.7** Tracer diffusion coefficients obtained in modeling vacancy diffusion in FCC phases of pure Al (gray circles), Al-2Zr (green triangles) and Al-5Zr alloy (red triangles). Parameters of the Arrhenius treatment are indicated at the top. The inset shows temperature dependence of the diffusion coefficients ratio  $D_{\text{Zr}}/D_{\text{AlZr}}$  in different alloys.

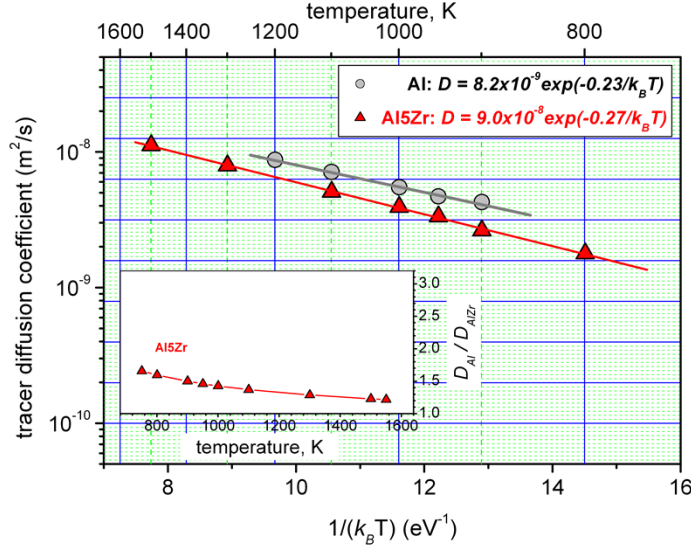


**Fig.8** Tracer diffusion coefficient obtained in modeling vacancy diffusion in melted phase of pure Al (gray circles) and Al-5Zr alloy (red triangles). Parameters of the Arrhenius treatment are indicated at the top. The inset shows temperature dependence of the diffusion coefficients ratio  $D_{Zr}/D_{AlZr}$ . The abscissa scale of the inset plot is the same as in Fig.4 for simplifying the visual comparison of diffusion coefficients ratio.

presented in Fig.7 together with the corresponding parameters of Arrhenius treatment in the inset table. The inset plot in Fig.7 shows the temperature dependence of the ratio  $D_{Al}^*/D_{AlZr}^*$ : the tracer diffusion coefficient in pure Al over that in Al-2Zr and Al-5Zr alloys. The data show that Zr additions decrease the total diffusivity in the alloy: 2at.% Zr reduces it by 20-50% whereas 5at.% Zr reduces the total diffusivity by 2-3 times depending on the temperature. Zr atoms also increase the effective activation energy for diffusion, 0.38 eV in pure Al and to 0.40 eV in the Al-5Zr alloy. Total tracer diffusivities in liquid phases of pure Al and Al-5Zr is shown in Fig.8 together with the corresponding parameters of an Arrhenius-type treatment (inset table). Like the solid phase, the addition of Zr decreases the total diffusivity. However, the effect is much weaker as seen in the inset plot in Fig.8. Also, the effective activation energy for diffusion in the alloy increases from 0.23 eV to 0.27 eV. Like in pure Al, diffusion in the liquid phase is much faster than in the FCC phase. This can be seen in Fig.9 where self-diffusion coefficients are shown as a function of the reciprocal temperature for solid and liquid phases of the Al-5Zr alloys. Note, that in estimating vacancy concentration in the FCC phase (see eq.(5)) we have used the vacancy formation value for pure Al (see Table. 1) and mono-vacancy formation entropy from [62]. In MD modeling we observed a region  $\sim 200\text{K}$  where both phases were stable over the modeling time. In this region,

self-diffusion in the melted phase is from four to five orders in magnitude faster than in the FCC phase. This is similar to that observed in pure Al (see Fig. 6).

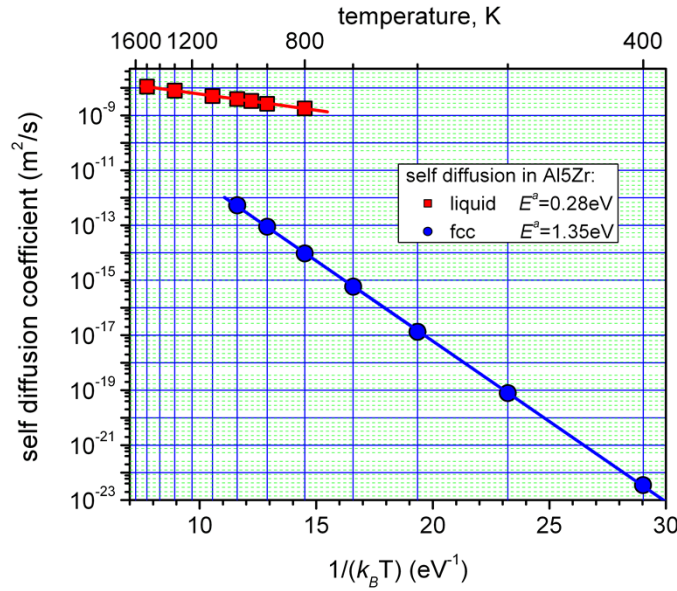


**Fig.9** Self diffusion coefficient obtained in modeling diffusion in melted (red squares) and FCC solid (blue circles) phases of Al-5Zr alloy

### 3.3. Al-25Zr alloy

The Al-25Zr alloy was modeled in three different states. First was  $L_{12}$ , a metastable intermetallic structure observed in precipitates before transforming into the stable  $DO_{23}$  [19]. With the IAPs used [26, 27] it has a high melting temperature,  $\sim 1600\text{K}$ , so we studied vacancy diffusion over the temperature range 1100-1600K. The second state was a random FCC solid solution that may appear after extremely fast solidification and during subsequent aging is expected to precipitate  $L_{12}$  or/and  $DO_{23}$  phases. This phase has a much lower melting temperature,  $\sim 1000\text{K}$ , so we studied vacancy diffusion over the temperature range 400-1000K. Finally, the third phase studied is the liquid Al-25Zr modeled over the temperature range 1100-1600K.

The results for solid phases are presented in Fig. 10 together with Arrhenius plots for pure Al, Al-2Zr and Al-5Zr alloys for comparison. The slowest diffusion is in the  $L_{12}$  phase which is also characterized by the highest effective activation energy,  $E^a=0.81\text{ eV}$ . Diffusion in the random Al-25Zr alloy, while being about an order in magnitude slower than that in Al and low-Zr alloys, has a similar activation energy,  $E^a=0.41\text{ eV}$ . Note that vacancy diffusion in the random Al-25Zr

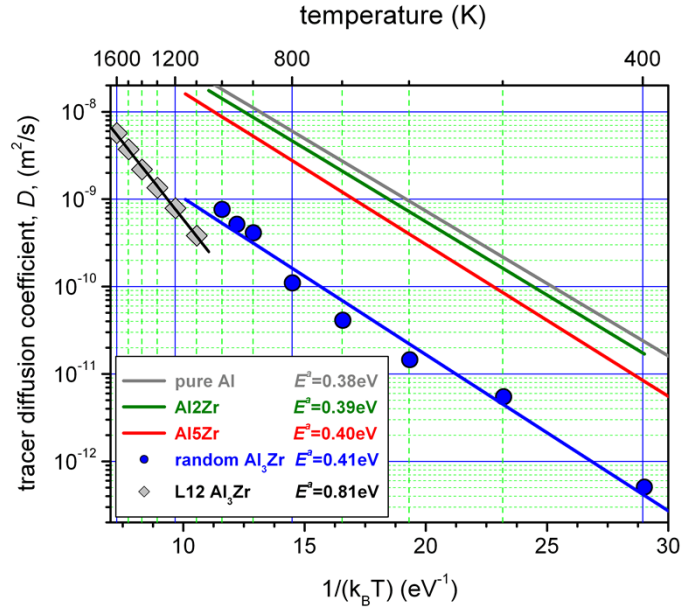


**Fig.10** Tracer diffusion coefficients obtained in modeling vacancy diffusion in Al-25Zr alloys in L<sub>12</sub> phase (gray diamonds), and in the FCC random alloy (blue circles). Green and red lines are Arrhenius plots for FCC pure Al and Al-5Zr alloy respectively.

alloy differs from that in other solid phases. This alloy is unstable, and immediately after its construction suffers local structural and chemical ordering that depend on the local distribution of Zr atoms and temperature. Such local ordering includes formation of L<sub>12</sub> embryos with slightly different orientations according to the local distribution of Zr atoms. As a result, the crystal volume becomes a nonhomogeneous structure where the local cohesive energy has a wide distribution, and some sites act as vacancy traps. This process slows down vacancy diffusion, especially at low temperatures. The time necessary to equilibrate the microstructure increases significantly, beyond the affordable MD modeling time, and therefore, cannot be taken as steady-state stationary diffusion as in the other cases.

Diffusion in the liquid Al-25Zr phase is also suppressed relative to the pure Al and low-Zr alloy (Fig.11). Like in the solid phases, increasing Zr concentration causes an increase of the effective activation energy: from 0.23eV in pure Al, through 0.27eV in the Al-5Zr alloy, to 0.49eV in the Al-25Zr alloy.

### 3.4. Chemically biased diffusion and alloy ordering

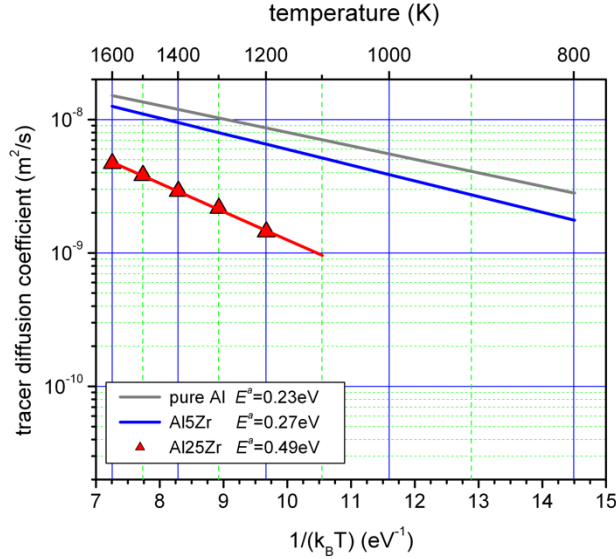


**Fig.11** Tracer diffusion coefficients obtained in modeling diffusion in the melted Al-25Zr alloy (red triangles). Black and blue lines are Arrhenius plots for melted pure Al and Al-5Zr alloy respectively.

The formation of Al<sub>3</sub>Zr layers during the aging of Al-Zr pairs unambiguously demonstrates that they are formed due to interdiffusion [15, 16]. The driving force for this transformation is the difference in chemical potentials and other parameters along the transformation pathway (e.g. vibrational and entropy properties, interfacial energy) that are minimized in the ordered intermetallic structures such as L1<sub>2</sub> and DO<sub>23</sub>. The diffusional formation of ordered structures, i.e., diffusional phase transformations, should be accompanied by changing local chemical order which can be estimated for all atoms via eq. (6). In practice, to obtain a detectable change of the CSRO parameter,  $\alpha_{ZrZr}^k$ , significant atomic rearrangements should be modeled. Note that this condition is satisfied in the liquid phase, where diffusivity is high and all atoms have long trajectories, but not in solid phases modelled here, where only one vacancy is migrating and long modeling times are required. Therefore, the accuracy of the ordering study in solids is much lower than that in the liquid phase.

Limited experimental data is available for either diffusion or defect energetics in Al-Zr. The only source [63] reported Zr impurity diffusion parameters in crystal Al as  $D_0 = 7.28 \times 10^{-2} \text{m}^2/\text{s}$  and  $E^a = 2.51 \text{eV}$  and compared Zr with other impurities including Au, Cu, Mg and Zn. Zr has the maximum diffusion activation energy and the minimum diffusion coefficient which, even at near

pre-melting temperature, is about three to four orders in magnitude lower than that of other solutes reported in [63]. The vacancy formation contribution to the effective activation energy in Al-Zr is unknown.

Atomic transport occurs via diffusion of Al and Zr atoms and may be characterized by the partial tracer diffusion coefficients of solvent Al,  $D_{Al}$ , and solute Zr,  $D_{Zr}$ , for a given alloy composition, eq.(3). The Al-Zr system is far from an ideal solid solution, and more modeling and/or experimental efforts are necessary for complete description of interdiffusion in the Al-Zr system (see e.g. [64-66]). Nevertheless, partial diffusion coefficients in different phases and temperatures in the Al-Zr estimated here are useful for qualitative analysis of processes near solid/liquid transition states. The Arrhenius parameters of partial tracer diffusion coefficients,  $D_{Al}$  and  $D_{Zr}$ , are presented in Table 2 and Fig.12.  $D_{Al}$  and  $D_{Zr}$  were found to be strongly dependent on the alloy composition and state, as reflected by the difference of Arrhenius parameters, suggesting that the Al-Zr system is strongly non-ideal. The effective activation energy for Al migration in the FCC structure changes from 0.38eV in pure Al, through 0.40 eV in the Al-5Zr alloy, to 0.43 in the random Al-25Zr alloy. In the intermetallic  $L1_2$  structure the Al diffusion activation energy is even higher: 0.81eV. Interestingly, the effective energy for Zr atomic

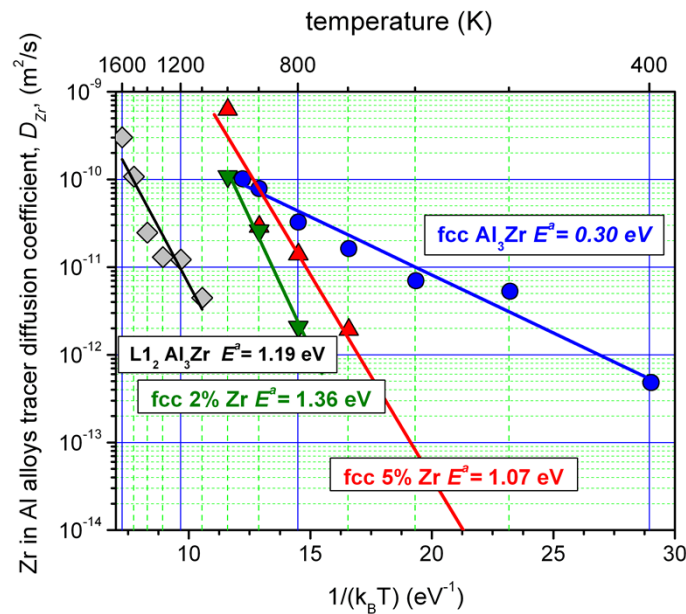


**Fig.12** Temperature dependence of Zr diffusion coefficients,  $D_{Zr}$ , in different alloys and structures. Insets indicate the corresponding activation energy.

migration in the random FCC Al-2Zr and Al-5Zr alloys and the L<sub>12</sub> structure of the Al-25Zr alloy is similar, i.e. 1.07 eV, 1.36 eV and 1.19 eV. However the pre-exponential factors differ by orders in magnitude:  $8720 \times 10^{-7}$  m<sup>2</sup>/s,  $720 \times 10^{-7}$  m<sup>2</sup>/s and  $7.95 \times 10^{-7}$  m<sup>2</sup>/s for the same cases. Correspondingly, the solute diffusion coefficient in the random Al-5Zr alloy is about two orders in magnitude higher than that in the L<sub>12</sub> Al<sub>3</sub>Zr intermetallic alloy. Slow diffusion of Zr in the L<sub>12</sub> structure of the Al-25Zr alloy is consistent with earlier observations in L<sub>12</sub> compounds, for example slow Al diffusion was observed in Ni<sub>3</sub>Al [68].

The Al-25Zr alloy having a random FCC structure provides high solute diffusivity with the lowest activation energy observed here in all solids:  $E^a = 0.30$  eV. As mentioned above, the random FCC Al-25Zr alloy is structurally unstable, diffusion process modeled here is in fact the chemical ordering and diffusional phase transformation towards the L<sub>12</sub> structure. Despite the fast Zr diffusion, over the modeling time here, we could neither detect clear transformation of the initial FCC structure, nor significant chemical ordering. Therefore, we describe this as a slow diffusional transformation and chemical ordering *towards* the L<sub>12</sub> phase.

Phase	Temperature range, K	$D_0$ , $10^{-7}$ m <sup>2</sup> /s	$E^a$ , eV	$D_{Al}^0$ , $10^{-7}$ m <sup>2</sup> /s	$E_{Al}^a$ , eV	$D_{Zr}^0$ , $10^{-7}$ m <sup>2</sup> /s	$E_{Zr}^a$ , eV
<b>Vacancy in solid</b>							
FCC Al	400 – 1000	15.2	0.38				
FCC Al-2Zr	400 – 1000	12.2	0.39	12.5	0.39	$8.72 \times 10^3$	1.36
FCC Al-5Zr	400 – 1000	9.26	0.40	9.91	0.40	720	1.07
FCC Al-25Zr	400 – 950	0.633	0.41	0.966	0.43	0.0361	0.30
L <sub>12</sub> Al-25Zr	1200 – 1600	19.4	0.81	25.1	0.81	9.75	1.19
<b>Diffusion in liquid</b>							
Al	900 – 1200	0.818	0.23				
Al-5Zr	800 – 1500	0.897	0.27	0.911	0.27	0.666	0.30
Al-25Zr	1200 – 1600	1.64	0.49	1.73	0.48	1.42	0.51

Note: In solid phases, parameters of the tracer diffusion were calculated via eq.(1), e.g. diffusivity per vacancy. In melted phases, tracer diffusion coefficients were normalized per number of modeled atoms ( $N_a = 4000$ ). For alloys, three sets of Arrhenius parameters are presented: total tracer diffusion coefficient  $D_0$ , Al tracers  $D_{Al}$  and Zr tracers  $D_{Zr}$  (see eq.(3)).

**Table 2** Diffusion parameters in different phases.

In most cases studied here,  $D_{Al}/D_{Zr} > 1$ , demonstrating that the diffusivity of Al atoms is always faster than that of Zr atoms with the exception of low-temperature diffusion in the random FCC Al-25Zr alloy. As shown in Fig. 13, the largest ratio, and, correspondingly, the lowest Zr mobility, is observed in the Al-25Zr alloy with  $L1_2$  structure. This result is not surprising as minor element diffusion in the stoichiometric  $L1_2$  structure is generally very slow (see e.g. [68]). The temperature dependence of the  $D_{Al}/D_{Zr}$  ratio is different for different phases and structures. In the  $L1_2$  and low-Zr random FCC alloys, this ratio decreases with increasing temperature. However, a random Al-25Zr FCC alloy behaves qualitatively differently:  $D_{Al}/D_{Zr}$  increases from  $\sim 0.5$  at low T to  $\sim 10$  just below the melting temperature. This means at low T, Zr moves faster than Al and it can be explained by the intensive chemical ordering discussed above. Despite the small ratio of  $D_{Al}/D_{Zr}$ , the absolute values of  $D_{Al}$  and  $D_{Zr}$  in this alloy are low (see Fig. 12), meaning the growth and coarsening of the  $L1_2$  structure is expected to be slow. For the low-Zr random FCC alloys, Zr

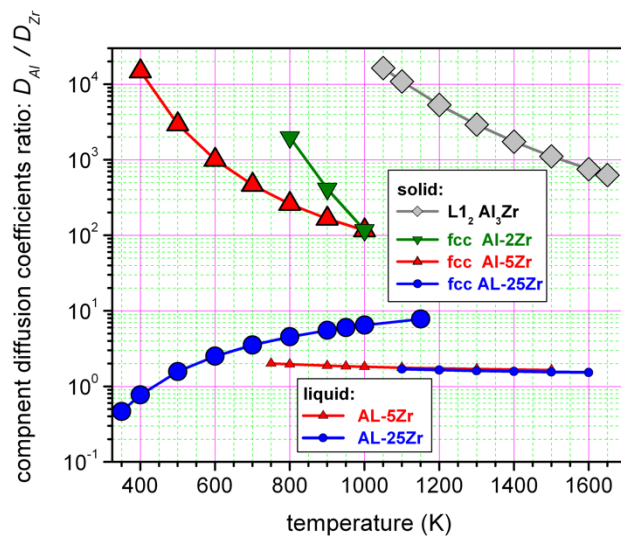


**Fig.13** Temperature dependence of ratio of component tracer diffusion coefficients  $D_{Al}/D_{Zr}$  obtained in modeling vacancy diffusion in the FCC and  $L1_2$  phases and diffusion in the melted phase of Al-5Zr and Al-25Zr alloys.

diffusion is negligible compared to that of Al diffusion. For example, at 1000K,  $D_{Al}/D_{Zr} \approx 100$

and the ratio increases by a few orders in magnitude at  $\sim 400\text{K}$ . A comparison between Al-2Zr and

Al-5Zr demonstrates that the Zr diffusivity is very different even in these relatively similar alloys.

The slow diffusion of Zr in stable FCC solid solution phase should suppress the growth and

coarsening of  $L_2$   $Al_3Zr$  or other intermetallic phases such as  $DO_{23}$   $Al_3Zr$ . Conversely, Zr diffusion

in liquid is: a) weakly temperature dependent, and b) does not depend on the composition. The

mean ratio  $D_{Al}/D_{Zr} \approx 2$  and, taking into account the factor that Zr atoms is >3 times heavier than

Al atoms, one can conclude that Zr diffusion is quite fast in liquid Al-Zr systems. Taking into

account that at comparable temperatures diffusion in the liquid state is a few orders in magnitude

faster than in the solid (Figs.11 and 12), and the difference in chemically biased diffusion shown

in Fig.13, one may expect that steady state ordering occurs much faster in the melted state. Indeed,

this trend was observed when studying the evolution of the CSRO parameters  $\alpha_{ZrZr}^k$  in alloys for

different conditions. The CSRO parameters in the liquid Al-5Zr alloy at 800K and 1000K are

presented in Fig. 14. In both cases a certain order in the Zr distribution was established when  $\alpha_{ZrZr}^1$

and  $\alpha_{ZrZr}^3$  are both positive, whereas  $\alpha_{ZrZr}^2$  is negative. This means that the Zr population in the

first and third coordination spheres of Zr atoms is higher than that in the random alloy, whereas

that in the second coordination is the opposite. These distributions were established quickly with

stable oscillations near values:  $\alpha_{ZrZr}^1 = 0.046$ ,  $\alpha_{ZrZr}^2 = -0.041$  and  $\alpha_{ZrZr}^3 = 0.023$  at 800K and

$\alpha_{ZrZr}^1 = 0.053$ ,  $\alpha_{ZrZr}^2 = -0.034$  and  $\alpha_{ZrZr}^3 = 0.023$  at 1000K. These values are slightly higher

than the corresponding CSRO parameters estimated for the perfect  $L_2$  structure:  $\alpha_{ZrZr}^1 = 0.030$ ,

$\alpha_{ZrZr}^2 = -0.011$ , and  $\alpha_{ZrZr}^3 = 0.011$ . Conversely, CSRO established during vacancy diffusion in

the FCC random solution was lower (Fig.15): the mean parameters saturate at:  $\alpha_{ZrZr}^1 = 0.006$ ,

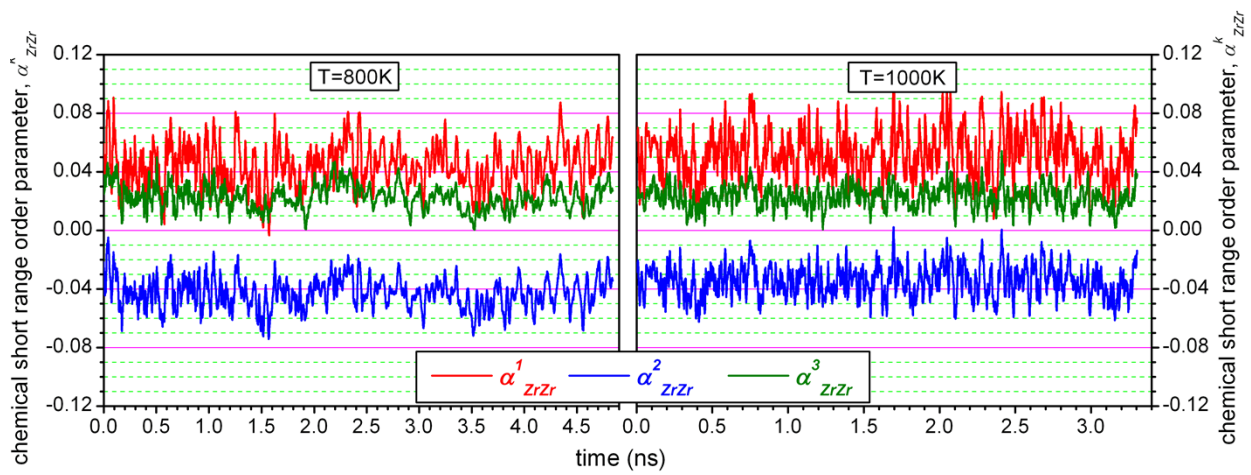


**Fig.14** Evolution of the modified chemical short range order parameters,  $\alpha_{ZrZr}^k$ , estimated by during modeling diffusion in Al5Zr melted phase at different temperatures.

$\alpha_{ZrZr}^2 = -0.015$  and  $\alpha_{ZrZr}^3 = 0.011$  at 800K, and  $\alpha_{ZrZr}^1 = 0.019$ ,  $\alpha_{ZrZr}^2 = -0.017$  and  $\alpha_{ZrZr}^3 = 0.015$  at 1000K. Note that for each state and temperature we compare CSRO created for the compatible total atomic square displacements, i.e. the compatible level of atomic rearrangements. For the liquid phase, the results are similar for different temperatures (see Fig.10) and demonstrated a converged ordering in both cases. In the Al-5Zr random FCC alloy, ordering at 800K, evolved slower than at 1000K. With the overall compatible atomic displacements, this can be explained by the strong temperature dependence of the  $D_{Al}/D_{Zr}$  ratio (Fig.10), i.e., the relative

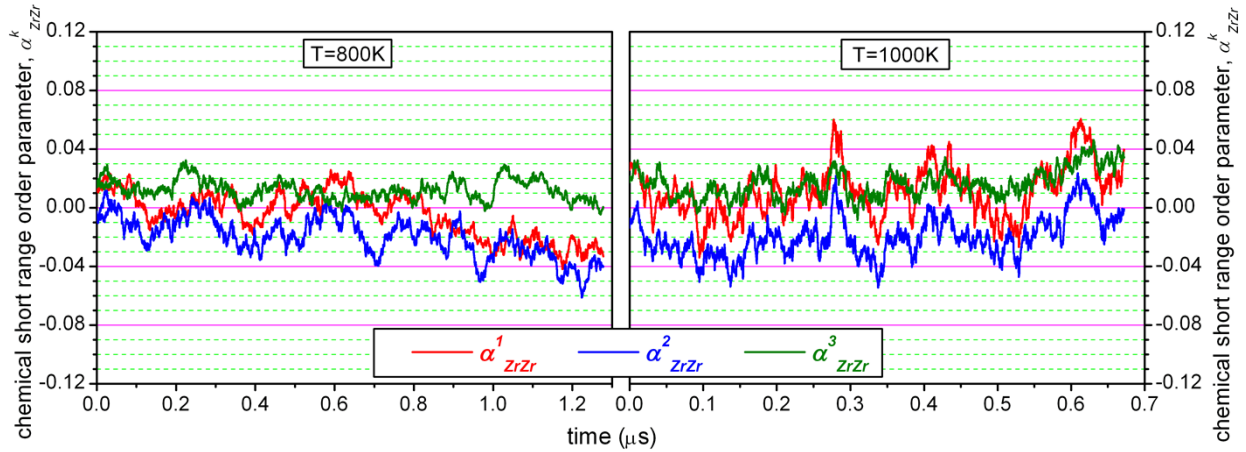


**Fig.15** Evolution of the modified chemical short range order parameters,  $\alpha_{ZrZr}^k$ , estimated during modeling vacancy diffusion in random FCC Al-5Zr alloy.

diffusivity of Zr increases more than two times when temperature increases from 800K to 1000K, which provides faster ordering at 1000K.

### **3.5 Non-Arrhenius behavior of diffusivity**

In the pure Al and Al-Zr alloys, nonlinear behavior of the tracer diffusion coefficient with

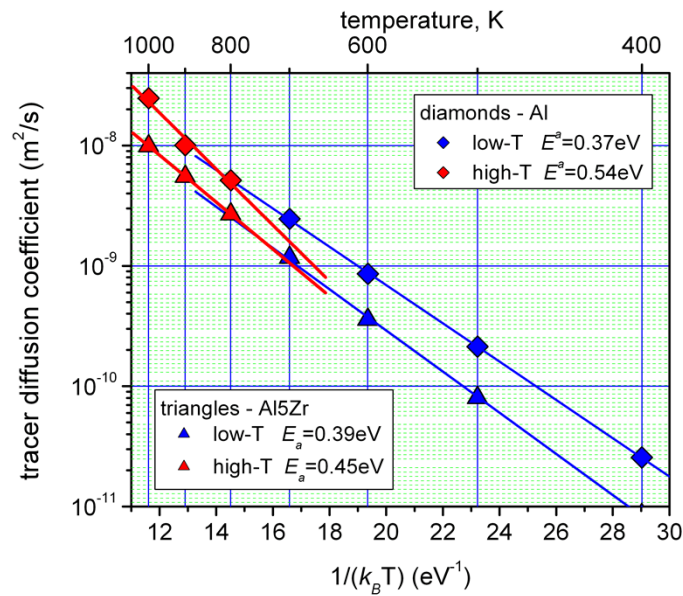


**Fig.16** Arrhenius-type plots and the corresponding activation energies for low- and high-temperature vacancy regions in pure Al and Al5Zr alloy.

reciprocal temperature was observed in the model results. Fig.16 shows examples for pure Al and

Al-5Zr with separate Arrhenius parameters for low- and high- temperature regions. Data for the

three highest temperatures in the range 800-1000K were treated as high-T, and in the range 400-

700K as low-T. Fig.16 shows a significant difference in high- and low- temperature slopes and the

corresponding activation energies define the level of difference: the effect is stronger in pure Al

than that in the Al5Zr alloy.  $E^a$  increases in pure Al from 0.37eV to 0.54eV with increasing

temperature whereas in the Al-5Zr alloy it increases from 0.39eV to 0.45eV. To elucidate the

mechanism for non-linear behavior, defects were analyzed during vacancy diffusion and in the

initially perfect Al FCC crystal. At high enough temperatures, short-lifetime pairs of vacancy and

interstitial atom, i.e. Frenkel pairs (FP), were formed. For statistical treatment, on-the-fly Wigner-Seitz cells (WSCs) were evaluated near each lattice site. Empty and two-atom WSCs detected simultaneously were used to define FP formation. FPs form due to the large amplitude of vibration of Al atoms, and their formation frequencies and lifetimes depend on temperature and composition. Most FPs annihilate immediately and may be considered large fluctuations in atomic displacements. However, in some cases, interstitials perform a few displacements before annihilation thus contributing to additional atomic displacements responsible for non-Arrhenius behavior. A recognizable and statistically significant concentration of defects in the perfect Al was observed only near the melting temperature, at 950K-1000K, whereas in Al-5Zr alloys FPs were observed down to 800K. The frequency and lifetime of individual FPs were not analyzed but their average concentration was estimated as a function of temperature (Fig.17). The highest activation

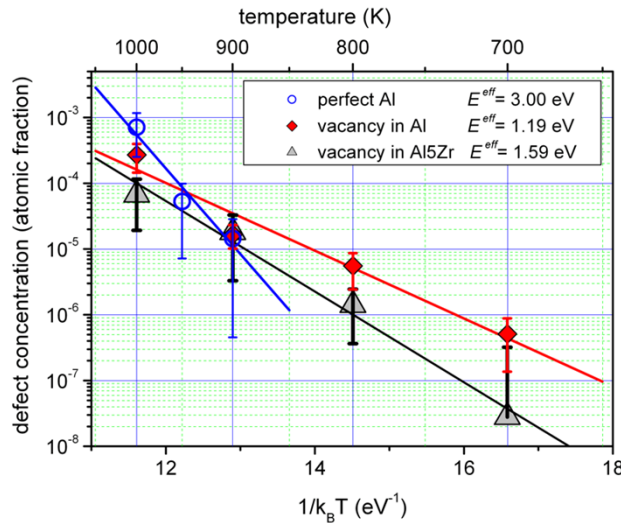


**Fig.17** The mean and standard deviation of Frenkel-pair concentration detected during evolution of initially perfect Al (blue open circles) and vacancy diffusion in pure Al (red diamonds) and Al-5Zr (grey triangles) alloy, their Arrhenius-like treatment (blue, red and gray lines) with the corresponding activation energies (in the inset) in pure Al and Al5Zr alloy.

energy,  $E^{eff}=3.00\text{eV}$  was obtained in the initially perfect Al. It decreased to 1.19 eV in the presence of a pre-existing vacancy. In the Al-5Zr crystal with a pre-existing vacancy  $E^{eff}=1.59\text{ eV}$ . These energies are related to formation of unstable objects with short lifetimes but cannot be attributed to the formation energy of particular defects. Note that the FPs formed in the studied temperature range and modeling time are unstable and annihilate athermally when the crystal is quenched and relaxed.

## 4. Discussion

The purpose of this research was understanding atomic-level mechanisms that affect diffusion-driven transformations at high cooling rates during additive manufacturing. Here, we report results on diffusion, atomic transport, and ordering in Al-Zr alloys. Such information is necessary to perform even qualitative predictions of phase transformations in practical additive manufacturing scenarios. Due to a lack of experimental and other modeling information on Al-Zr system, the present results are a unique source of at least part of the necessary information.

### 4.1 Specific features of diffusion and atomic transport in pure Al and AlZr alloys

First, we underline the accuracy of the present modeling results. As demonstrated in the Section 2.2, the modeling time scale provides good convergence of the diffusional data. Convergence of the alloy ordering processes depended on the state: rapid convergence was achieved in the liquid, but solid solutions, especially the structurally unstable FCC random Al-25Zr alloy, demanded longer modeling times. Diffusional ordering and transformations in some solid states are still an open challenge.

Some modeling [47] and experimental [48, 49] studies in Al observed non-Arrhenius diffusion behavior at high temperatures and have proposed different mechanisms. MD modeling in [47] reported double jumps of a vacancy that accelerated atomic displacements at high T. Analysis of quenching and annealing and nuclear magnetic resonance experiments in [48] reported estimated energy properties of possible di-vacancies: migration 0.41 eV and binding 0.14eV. Modeling of vacancy diffusion in Al and Al-Zr alloys performed here allowed the detection of non-Arrhenius behavior near pre-melting temperatures and interrogation of the controlling mechanism. Acceleration of tracer diffusivity at high T and the corresponding increase in the diffusion activation energy observed in this research is demonstrated in Fig.16. The effect is more significant in pure Al than in the Al-5Zr alloy. On-the-fly analysis of Wigner-Seitz cells detected formation of Frenkel-pair like defects. We observed that these FPs have a short lifetime for the “vacancy” and “interstitial” are not enough separated and mostly recombine just after a short time they are formed. These defects are formed due to large fluctuations in the displacement of certain

Al atoms from their lattice sites that creates a temporal empty site (vacancy) and an “interstitial-like” defect nearby. Depending on the temperature an “interstitial” may perform a few jumps before it recombines with the “vacancy”, thus producing additional atomic displacements that contribute to acceleration of the Al tracer diffusivity. The effective energy of these defects’ formation obtained in pure, initially perfect, Al (3.00eV, Fig.17), is close to 3.17eV - the formation energy of a stable Frenkel pair: a vacancy and <100> dumbbell separated by  $\sim 8a$  as modelled in pure Al. Addition of a pre-existing vacancy decreases  $E^{eff}$  down to 1.19 eV in pure Al and to 1.59 eV in Al-5Zr. The separation of “vacancy” and “interstitial” is short, just one-two interatomic distances, and during quenching, they always recombine. This is the feature of Al and Al-rich alloys where, due to the low mass of atoms, such fluctuations can occur at relatively low temperatures, well below the melting. In the perfect Al lattice the obtained value of  $E^{eff}$  demonstrates a clear similarity with Frenkel pairs formation. A significantly lower value in non-perfect Al and alloys suggests that the observed defects, created near vacancies and/or impurities with much lower formation energy, cannot be attributed to conventional Frenkel defects. More complicated mechanisms involving locally correlated atomic displacements around defects occur here. We did not investigate these mechanisms in details but assume that some of them are similar to recently observed atomic chains and displacement loops reported in [69]. Above the melting temperature, vacancies and interstitials forming these defects can be separated enough to initiate homogenous melting.

#### 4.2 Zr effect to diffusion and atomic transport in AlZr alloys

As was demonstrated unambiguously here, the addition of Zr reduces the total diffusivity and slowdown atomic transport in Al-based alloys. The effect is stronger in solid than liquid phases. Addition of 5at.% Zr decreases the tracer diffusivity in FCC alloy by 2-3 times and only  $\sim 1.5$  times in its liquid state. The applied IAPs underestimate vacancy - Zr solute interactions compared to DFT modeling. DFT reports strong repulsion in the first coordination: binding energy  $E_{V-Zr_1}^b = -0.352\text{eV}$ , whereas IAPs reproduce practically no interaction with  $E_{V-Zr_1}^b = 0.004\text{eV}$  (see Table 1). Weaker repulsion means that the current IAPs most probably underestimate the decelerating effect of Zr solute in the overall diffusion in Al-Zr solid solutions. Nevertheless, in all studied Al-Zr alloys and phases, we have observed deceleration of the total tracer diffusivity and slow diffusion of Zr atoms. An especially large ratio of the component’ tracer diffusion

coefficients,  $D_{Al}/D_{Zr}$ , was observed in all structurally stable solid states. Thus, in the FCC Al-5Zr alloy this ratio was between  $\sim 10^4$  and  $\sim 100$  for the temperature range 400 - 1000K. In the same liquid alloy,  $D_{Al}/D_{Zr} \approx 1.5$  and was almost constant over the temperature range 900-1500K. In the more concentrated alloy, Al-25Zr, Zr diffusion was minimal in the  $L1_2$  phase (Fig.12), and the ratio is maximal (Fig.13). However, the effect was weaker in the FCC random alloy :  $D_{Al}/D_{Zr} \approx 0.8-8$  over the temperature range 400-1100K. Therefore, in this alloy Zr diffusion can be even accelerated at low temperature, and just slightly decelerated above  $\sim 450$ K. The random FCC Al-25Zr alloy was structurally unstable and suffered chemical ordering and structural transformation towards the more stable  $L1_2$  and/or  $DO_{23}$  phases. During vacancy diffusion in the initially random Al-25Zr alloy, we observed significant atomic transport and intensive local transformations, when a few tens of atoms created a domain with a slightly different chemical order and orientation relative to the initially random matrix. However, complete transformation towards any of the intermetallic phases was not observed at any temperature because the diffusional transformation needs a much longer time than the microsecond scale in this study.

Qualitative effects of slow Zr diffusivity in Al solid solution were also observed experimentally. The comparison of solute diffusivities in Al presented in [63] demonstrates that Zr diffusivity by a few orders in magnitude is lower than any other considered cases. Quantitative comparison of diffusivities of Sc and Zr in Al was made in [70] and the conclusion made that at 723K Sc is  $\sim 1000$  times faster than Zr, is consistent with the data presented in [63]. Taking into account that Sc is much slower than Al, as was stated in [63, 70], the ratio  $D_{Al}/D_{Zr} \approx 300-2000$ , obtained here at  $T=800$ K in Al-2Zr and Al-5Zr alloys, appears very reasonable.

The component tracer diffusivities,  $D_{Al}$  and  $D_{Zr}$ , can be used in estimating the chemical diffusion coefficient,  $\tilde{D}$ , in Darken's formulation [65, 66]:

$$\tilde{D} = (C_{Zr}D_{Al}^* + C_{Al}D_{Zr}^*)\Phi, \quad (7)$$

where  $\Phi = 1 + \frac{\partial \ln(\gamma_{Al})}{\partial \ln(C_{Al})}$  is a thermodynamic factor and  $\gamma_{Al}$  is the activity coefficient of the solute (Zr) in matrix (Al), that defines how far is the Al-Zr system from the ideal solution.  $\gamma_{Al}$  is structure, composition and temperature dependent and usually obtained by fitting theory or modeling to experimental diffusion profiles. An example of  $\gamma_{Al}$  values for some transition metals in Al is presented in [71]:  $\gamma_{Al-Fe}=0.24-0.90$  ( $T < 1173$ K),  $\gamma_{Al-Ni} \approx 0.5$  ( $400\text{K} < T < 1500\text{K}$ ) and  $\gamma_{Al-Ti}=0.25-0.89$  ( $T < 1700$ K).  $\gamma_{Al}$  values for the same liquid alloys are usually below 1.0 at  $T < 2000$ K [72]. We

did not find any published data on the activity coefficients for the solid Al-Zr system. As far as the diffusion in liquid Al-Zr systems is concerned, we have found only one *ab initio* MD study [73] where compositions several AlZr compositions were modelled. The closest composition to the studied here  $\text{Al}_3\text{Zr}$ , in [73] was  $\text{Al}_3\text{Zr}_2$  for which the activation energies for Al and Zr diffusion were where found to be equal to  $\sim 0.56$  eV and  $\sim 0.59$  eV correspondingly. These values are rather close to 0.48 eV and 0.51 eV defined here for  $\text{Al}_3\text{Zr}$  (see Table 1). The ratio  $D_{\text{Al}} / D_{\text{Zr}} \sim 1.75$  obtained in [73] in  $\text{Al}_3\text{Zr}_2$  is also close to the value  $\sim 1.5-2.0$  obtained here in  $\text{Al}_3\text{Zr}$  (see Fig.13).

### 4.3 Chemical ordering by diffusion in AlZr alloys

Specific diffusion behavior of Zr in AlZr alloys defines the features in the chemical ordering process and its rate occurring in different phases. Zr diffusion is suppressed in all structurally stable solid Al-Zr phases compared to diffusion in the liquid state. This, together with the fact that self-diffusion in the liquid state is a few orders in magnitude faster than that in solid states (Figs.8-10), leads to significantly faster ordering in the liquid state in the Al-Zr system. This effect is reproduced by atomistic modeling and can be seen by comparing plots for the evolution of chemical short-range order parameters,  $\alpha_{\text{ZrZr}}^k$  (Figs. 11 and 12) for the Al-5Zr alloy. Chemical ordering in the melted Al-Zr alloys occurs quickly and the ordering level weakly depends on the temperature. That means that at a wide range of conditions at the melting stage during the additive manufacturing process one may expect a clear order in the Al-Zr alloy before its solidification. These are not compact Zr-precipitates but loose clouds with a few atomic percent excess in local concentration of Zr. For example, Fig.15 demonstrates that at 1000K among the first neighbors there are about 3% more Zr atoms than in the random state. Among the second neighbors, the situation is the opposite and these are depleted in Zr by  $\sim 4\%$ . However, all three neighbor spheres are overall enriched with Zr at about 3% over the random state. During fast cooling and solidification, the chemical order will be kept in the undercooled state ahead of the moving solid-liquid interface, as we observed during modeling diffusion at temperatures below the melting point in the considered here systems (e.g. Fig.15 at 800K). It is important to note that this is chemical short order, but not structural for it is related to the liquid phase. Zr-rich regions, having higher solidification temperature, should solidify earlier to form  $\text{L1}_2$  or  $\text{DO}_{23}$  precipitates which may serve as nucleation sites for FCC dendrites. Experiments show that  $\text{L1}_2$   $\text{Al}_3\text{Zr}$  precipitates formed

first in rapidly solidified alloys with 5-15 at.% Zr and the consequent transformation towards DO<sub>23</sub> precipitates during annealing at the temperatures 573-773K [19]. Ageing Al-Zr couples, see e.g. [15-18], does not proceed through the solidification stage but evolves under more thermodynamically stable conditions. This evolution misses nucleation of L1<sub>2</sub> phase and DO<sub>23</sub> nucleates and grows directly due to its higher stability.

#### 4.4 Diffusion mediated evolution of AlZr alloys in crystal and liquid states

The results on atomic transport and ordering obtained here allow us to suggest the following scenario when L1<sub>2</sub> can be stabilized in low Zr-concentration alloys. Fast cooling in additive manufacturing conditions stabilizes the FCC structure with a certain CSRO formed already in the liquid phase. Just after solidification, diffusional phase transformation towards a structurally ordered phase occurs heterogeneously depending on the local chemical composition and order. The simplest ordered Al<sub>3</sub>Zr phase is L1<sub>2</sub> which is completely coherent with the FCC matrix and is just slightly less stable than the ground state DO<sub>23</sub> phase (see Table A1). A certain chemical order achieved in the liquid phase needs to be diffusively transformed into structural order of the stable intermetallic phases. The corresponding diffusion rate can be very high due to several specific phenomena. For example, a) local excess free volume due to lower equilibrium volume after solidification (see Fig.1) provides a high vacancy concentration, b) accelerated diffusion due to increased defect concentration near pre-melting temperatures (non-Arrhenius effects considered in Section 3.5), and c) structural instability of random FCC alloys with high Zr concentration (see Sections 3.3 and 3.4). These mechanisms affect the local diffusion and structural transformation towards compact intermetallic structures just after solidification. The L1<sub>2</sub> phase, being coherent with FCC, has a higher probability of formation first via chemical reordering within the existing FCC phase. Further transformation towards DO<sub>23</sub> requires additional atomic displacements due to more complicated chemical order and lattice structure, but the driving force for this transformation is low due to a small difference in cohesive energy (see Table A1). Moreover, this transformation occurs under fast cooling conditions. If the temperature drops fast enough below the mobility of Zr atoms, already formed L1<sub>2</sub> precipitates can be stabilized. Fast cooling is therefore necessary to stabilize coherent L1<sub>2</sub> and prevent their further growth and diffusional transformation towards DO<sub>23</sub> (e.g., as was observed in [19]). In high Zr-concentration alloys, L1<sub>2</sub> precipitates can be formed directly during solidification [74]. Subsequent evolution

depends on the cooling rate, diffusion rate and driving force for  $L1_2$ -to- $DO_{23}$  transformation, that, in turn depends on their relative stability. In the Al-Zr system, where  $DO_{23}$  is just slightly more stable than  $L1_2$  and the diffusion rate is low,  $L1_2$  can be stabilize over a wide range of AM conditions.

The distribution and size of  $L1_2$  precipitates are expected to be controlled by the cooling rate for it affects the distribution of chemically ordered regions at the liquid phase just before solidification and nucleation and the growth of the structurally ordered phase just after solidification. Comparing to the cooling rate of conventional casting in the range of 1~100K/s, the cooling rate of additive manufacturing can go as high as  $10^7$ K/s. The specific thermal conditions at the solid-liquid interface are heavily influenced by parameters during the AM process, such as the laser power and speed. Composition gradients that form in front of the liquid/solid interface and which affect the nucleation and growth of crystalline phases from liquid and subsequent microstructure evolution, are dependent on the kinetics of diffusion in the liquid near this interface. Therefore the current study on the diffusion in liquid provides a critical parameter to simulate the concentration profile in front of solid/liquid interface, which is essential to understand the solidification microstructure relevant rapid solidification of AM. Further modeling activity towards more precise control of these processes during additive manufacturing is focused on the understanding of the distribution of chemically ordered phases in the liquid state and liquid/solid interface, their solidification and structural transformation, and how cooling condition affect these phenomena.

## 5. Conclusions

- An extended atomistic modeling of diffusion and atomic transport has been performed in solid random and ordered alloys and liquid phases of Al-Zr system with different compositions. Total and partial diffusion coefficients were obtained in different states.

- A strong decelerating effect of Zr in Al-based alloys was observed that accompanied with a chemical bias effect: depending on temperature Zr diffuses  $\sim 10^2$ - $10^4$  time slower than Al.

- Deceleration and chemical bias effects are much weaker in the liquid state, where they are also practically temperature independent.

- Chemical ordering saturates very quickly in the liquid state. Microsecond modeling scale did not lead to a significant ordering in solid phases.

- The results are discussed in view of optimizing the additive manufacturing parameters for the controlled formation of metastable  $L1_2$  precipitates.

**Acknowledgements.** This research is sponsored by the Laboratory Directed Research and Development Program of Oak Ridge National Laboratory, managed by UT-Battelle, LLC, for the US Department of Energy.

**Author Contributions.** Y.O. and Y.Y. conceived the idea, Y.O. performed MD modeling, data treatment, and drafted the manuscript, A.P. provided links to higher-level modeling and performed theoretical analysis, Y.Y. performed the analysis of experimental results and managed the project. All the authors contributed to the discussion of the project and manuscript preparation.

**Data Availability.** The authors declare that most data supporting the findings of this study are available within the paper. Requests for materials, including data that support the plots and other findings of this study, are available from the corresponding author upon a reasonable request.

**Declaration of Interests.** The authors declare no Competing Financial or Non-Financial Interests.

## References

1. Pollock, T. M., Tin, S. Nickel-based superalloys for advanced turbine engines: chemistry, microstructure and properties. *J. Propuls. Power*, **22**, 361 (2006).
2. Knipling K.E., Dunand D.C., Seidman D.N., Criteria for developing castable, creep-resistant aluminum-based alloys – a review. *Zeitschrift für Metallkunde*. **97**, 246 (2006).
3. M. J. Aziz, Model for solute redistribution during rapid solidification, *Journal of Applied Physics*, **53**, 1158 (1982).
4. Kurz, W, Giovanola, B., Trivedi, R., Theory of microstructural development during rapid solidification, *Acta Metall.*, **35**, 823 (1986).
5. Bathula, V., Liu, C., Zweiacker, K., McKeown, J., Wiezorek, J.M.K., Interface velocity dependent solute trapping and phase selection during rapid solidification of laser melted hypo-eutectic Al-11at.%Cu alloy, *Acta Mater.*, **195**, 341 (2020).
6. Todeschini, P., G. Champier, and F. H. Samuel, Production of Al-(12–25) wt% Si alloys by rapid solidification: melt spinning versus centrifugal atomization, *J. of Mater. Sci.*, **27**, 3539 (1992).
7. Michi, R.A., Plotkowski, A., Shyam, A., Dehoff, R., and Babu, S.S., Towards high-temperature applications of aluminium alloys enabled by additive manufacturing, *Intern. Mater. Reviews*, **67**, 298 (2022).
8. Glerum, J.A., Kenel, C., Sun, T., and Dunand, D.C., Synthesis of precipitation-strengthened Al-Sc, Al-Zr and Al-Sc-Zr alloys *via* selective laser melting of elemental powder blends, *Additive Manufacturing*, **36**, 101461 (2022).
9. Croteau, J.R., Griffiths, S., Rossell, M.D., Leinenbach, C., Kenel, C., Jansen, V., Seidman, D.N., Dunand, D.C., Vo, N.Q., Microstructure and mechanical properties of Al-Mg-Zr alloys processed by selective laser melting, *Acta Mater.*, **153**, 35 (2018).
10. Bahl, S., Sisco, K., Yang, Y., Theska, F., Primig, S., Allard, L.F., Michi, R.A., Fancher, C., Stump, B., Dehoff, R., Shyam, A., Plotkowski, A., Al-Cu-Ce(-Zr) alloys with an exceptional combination of additive processability and mechanical properties, *Additive Manufacturing*, **48**, 102404 (2021).

11. Wołczyński, W., Krajewski, W., Ebner, R., and Kloch, J., The use of equilibrium phase diagram for the calculation of non-equilibrium precipitates in dendritic solidification. *Theory. CALPHAD*, **25**, 401 (2001).
12. Aziz, M. J., Model for solute redistribution during rapid solidification. *Journal of Applied Physics*, **53**, 1158 (1982).
13. Knipling, K.E., Dunand, D.C., Seidman, D.N., Nucleation and Precipitation Strengthening in Dilute Al-Ti and Al-Zr Alloys, *Metall Mater Trans A*, **38**, 2552 (2007).
14. Knipling, K.E., Dunand, D.C., Seidman, D.N., Precipitation evolution in Al-Zr and Al-Zr-Ti alloys during isothermal aging at 375–425 °C, *Acta Mater.*, **56**, 114 (2008).
15. Kidson, G.V., Miller, G.D., A study of the interdiffusion of aluminum and zirconium, *J. Nucl. Mater.*, **1**, 61 (1964).
16. Laik, A., Bhanumurthy, K., Kale, G.B., Intermetallics in the Zr-Al diffusion zone, *Intermetallics*, **12**, 69(2004).
17. Dezellus, O., Gardiola, B., Andrieux, J., On the Solubility of Group IV Elements (Ti, Zr, Hf) in Liquid Aluminum Below 800°C. *J. of Phase Equilibria and Diffusion*, **35**, 120 (2014).
18. Souza, P.H.L., Quaresma, J.M.V, Oliveira, C.A.S., Precipitation Evolution and Modeling of Growth Kinetics of L1<sub>2</sub>-structured Al<sub>3</sub>Zr Particles in Al-0.22Zr and Al-0.32Zr (wt.%) Alloys Isothermally Aged, *Mat. Res.* **20** (2017). ([10.1590/1980-5373-MR-2017-0481](https://doi.org/10.1590/1980-5373-MR-2017-0481)).
19. Guo, J.Q., Ohtera, K., An intermediate phase appearing in L1<sub>2</sub>-Al<sub>3</sub>Zr to DO<sub>23</sub>-Al<sub>3</sub>Zr phase transformation of rapidly solidified Al-Zr alloys, *Materials Letters*, **27**, 343 (1996).
20. Clouet, E., Sanchez, J.M., First-principles study of the solubility of Zr in Al, *Phys. Rev. B* **65**, 094105 (2002).
21. Bo, H., Liu, D.D., Liu, L.B., Zhang, L.J., Du, Y., Xiong, X., Jin, Z.P., Computational study of atomic mobilities in Al-Zr solid solutions and the growth of ZrAl<sub>3</sub> intermetallic phase, *CALPHAD: Computer Coupling of Phase Diagrams and Thermochemistry*, **40**, 34 (2013).
22. Clouet, E., Nastar, M., Barbu, A., Sigli, C., Martin, G., An Atomic and Mesoscopic Study of Precipitation Kinetics in Al-Zr-Sc Alloys, *Advanced Engineering Materials*, **8**, 1228 (2006).
23. Clouet, E., Nastar, M., Barbu, A., Sigli, C., Nucleation of Al<sub>3</sub>Zr and Al<sub>3</sub>Sc in aluminum alloys: From kinetic Monte Carlo simulations to classical theory, *Phys. Rev. B* **69**, 064109 (2004).
24. Zhao, S., Osetsky, Y.N., Zhang, Y., Preferential diffusion in concentrated solid solution alloys: NiFe, NiCo and NiCoCr. *Acta Mater.* **128**, 391 (2017).

25. Osetsky, Y.N., Barashev, A.V., Zhang, Y., Sluggish, chemical bias and percolation phenomena in atomic transport by vacancy and interstitial diffusion in Ni-Fe alloys. *Current Opinion in Solid State and Materials Science*, **25**, 100961 (2021).
26. Cui, Y.Y., Wang, T.L., Li, J.H., Dai, Y., Liu, B.X., Thermodynamic calculation and interatomic potential to predict the favored composition region for the Cu–Zr–Al metallic glass formation, *Phys. Chem. Chem. Phys.*, **13**, 4103 (2011).
27. Bai, X., Li, J., Li, N., Luo, S., Liu, B.X., Prediction of Glass-Forming Ability and Atomic-Level Structure of the Al–Zr–Pd Metallic Glasses by Molecular Dynamics Simulations, *J. Phys. Soc. Japan*, **82**, 124006 (2013).
28. Kohn, W., Sham, L.J., Self-Consistent Equations Including Exchange and Correlation Effects, *Phys. Rev.* **140**, 1133 (1965).
29. Perdew, J. P., Burke, K., Ernzerhof, M., Generalized Gradient Approximation Made Simple, *Phys. Rev. Lett.* **77**, 3865 (1996).
30. Blöchl, P.E., Projector augmented-wave method, *Phys. Rev.* **B 50**, 17953 (1994).
31. Vienna Ab initio Simulation Package, <http://cms.mpi.univie.ac.at/vasp/>.
32. Lide, D.R, *CRC Handbook of Chemistry and Physics* (CRC Press, New York, 2002).
33. Hall, T.I., Goland, A.N., Snead Jr., C.L., Applications of positron lifetime measurements to the study of defects in metals, *Phys. Rev.* **B10**, 3062 (1974).
34. Furukawa, K., Takamura, J., Kuwana, N., Tahara, R., Abe, M., Quenched-In Vacancies in Aluminum, *Acta Cryst.* **A28**, 159 (1972)
35. Tzanetaki, P., Hillaire, J., Revel, G., The formation energy of vacancies in Aluminium and Magnesium, *phys. stat. sol.*, **75**, 433 (1976).
36. Feder, R., Nowzck, A.S., Use of Thermal Expansion Measurements to Detect Lattice Vacancies near the Melting Point of Pure Lead and Aluminum, *Phys. Rev.*, **109**, 1959 (1958).
37. Ghosh, G., Vaynman, S., Asta, M., Fine, M.E., Stability and elastic properties of L1<sub>2</sub>-(Al,Cu)<sub>3</sub>(Ti,Zr) phases: Ab initio calculations and experiments, *Intermetallics*, **15**, 44 (2007).
38. Osetsky, Y.N., Atomistic study of diffusional mass transport in metals. *Defects and Diffusion in Metals - Annual Retrospective III, 2001*, Defect and Diffusion Forum, **188-190**, 71 (2001).
39. Belashchenko, D.K., Computer simulation of liquid metals, *Physics – Uspekhi*, **56** (2013) 1176. (10.3367/UFNe.0183.201312b.1281).

40. Jakse, N., Pasture, A., Liquid Aluminum: Atomic diffusion and viscosity from ab initio molecular dynamics, *Sci. Reports*, **3**, 3135 (2013).
41. M. Leitner, T. Leitner, A. Schmon, K. Aaziz, and G. Pottlacher, Thermophysical Properties of Liquid Aluminum, *Metall. And Mater. Transactions*, 48A (2017) 3036.
42. Gautam, G., Kumar, N., Mohan, A., Mohan, S., Singh, D., ZrB<sub>2</sub> nanoparticles transmuting tribological properties of Al<sub>3</sub>Zr/ AA5052 composite, *J. Brazilian Soc., of Mech. Sci. and Eng.*, 41, 41 (2019).
43. Li, D-L., Chen, P., Yi, J-X., Tang, B-Y., Peng, L-M., Ding, W-J., Thermal Properties of the FCC Al<sub>3</sub>Zr : First-principles Study, *Mater. Sci. Forum*, **650**, 313 (2010).
44. Amador, C., Hoyt, J.J., Chakoumakos, B.C., de Fontaine, D., Theoretical and Experimental Study of Relaxations in Al<sub>3</sub>Ti and Al<sub>3</sub>Zr Ordered Phases, *Phys. Rev. Lett.*, **74**, 4955 (1995).
45. R.J.Kematick, H.F.Franzen, Thermodynamic study of the zirconium-aluminum system, *J. Solid State Chem.*, 54 (1984) 226.
46. Karin M. Carling, Goran Wahnstrom, Thomas R. Mattsson, Nils Sandberg, and Goran Grimvall. Vacancy concentration in Al from combined first-principles and model potential calculations, *Phys. Rev.*, B 67 (2003) 054101.
47. Da Fano, A., Jacucci, G., Vacancy Double Jumps and Atomic Diffusion in Aluminum and Sodium, *Phys. Rev. Lett.*, **39**, 950 (1977).
48. Seeger, A., Wolf, D., Mehrer, H., Analysis of Tracer and Nuclear Magnetic Resonance Measurements BY of Self-Diffusion in Aluminium, *Phys. Stat. Sol.*, b 48 (1971) 481.
49. Dias, S., Messer, R., Seeger, A., Nuclear-Magnetic-Resonance study of self-diffusion in aluminium, *Mat. Sci. Forum*, **15-18**, 419 (1987).
50. Li, Q.J., Sheng, H., Ma, E., Strengthening in multi-principal element alloys with local-chemical-order roughened dislocation pathways, *Nat. Commun.* **10**, 3563 (2019).
51. Lundy, T. S., Murdock, J.F., Diffusion of Al<sup>26</sup> and Mn<sup>54</sup> in aluminum, *J. Appl. Phys.*, **33**, 1671 (1962).
52. Federighi, T., A possible determination of the activation energy for self-diffusion in aluminium, *Philos. Mag.*, **4**, 502 (1959).
53. Volin, T. E., Balluffi, R.W., Annealing Kinetics of Voids and the Self-Diffusion Coefficient in Aluminum, *Phys. Stat. Sol.* 25, 163 (1968).

54. Burke, J., Ramachandran, T.R., Self-Diffusion in Aluminum at Low Temperatures, *Metallurg. Transact.*, **3**, 147 (1972).
55. Fradint, F. Y., Rowland, T. J., NMR measurement of the diffusion coefficient of pure aluminum, *Appl. Phys. Lett.*, **11**, 207 (1967) .
56. Stoebe, G., Gulliver, R. D., Ogurtani, T. O., Nuclear magnetic resonance studies of diffusion of Al<sup>27</sup> in aluminum and aluminum alloys, *Acta Metallurg*, **13**, 701 (1965).
57. Khellaf, A., Seeger, A., Emrick, R.M., Quenching Studies of Lattice Vacancies in High-Purity Aluminium, *Mater. Transactions*, **43**, 186 (2002).
58. Demmel, D. Szubrin, W.-C. Pilgrim, and C. Morkel, Diffusion in liquid aluminium probed by quasielastic neutron scattering, *Phys. Rev. B* **84**, 014307 (2011).
59. Kargl, F., Weis, H., Unruh, T., Meyer, A., Self diffusion in liquid aluminium, *Journal of Physics: Conference Series*, **340**, 012077 (2012).
60. Manga, V.R., Poirier, D.R., Ab initio molecular dynamics simulation of self-diffusion in Al–Si binary melts, *Modelling Simul. Mater. Sci. Eng.*, **26**, 065006 (2018).
61. Becker, C.A., Kramer, M.J., Atomistic comparison of volume-dependent melt properties from four models of aluminum, *Modelling Simul. Mater. Sci. Eng.* **18**, 074001 (2010).
62. Ju Yuan-Yuan, Zhang Qing-Ming, Gong Zi-Zhen and Ji Guang-F, Molecular dynamics simulation of self-diffusion coefficients for liquid metals, *Chin. Phys. B* **22**, 083101 (2013).
63. Hirano, K., Fujikawa, S., Impurity diffusion in aluminum, *J. Nucl. Mater.*, **69-70**, 564 (1978).
64. Carling, K.M., Wahnstrom, G., Mattsson, T.R., Sandberg, N., Grimvall, G., Vacancy concentration in Al from combined first-principles and model potential calculations, *Phys. Rev.*, **B 67**, 054101 (2003).
65. Darken, L.S. Diffusion, Mobility, and their interrelation through free energy in binary metallic systems. *Trans. AIME*, **175**, 184 (1948).
66. Mehrer, H., *Diffusion in Solids*, Springer-Verlag Berlin Heidelberg (2007): ISBN 978-3-540-71486-6.
67. Di Pietro Martínez, D., Hoyuelos, M., Diffusion in binary mixtures: An analysis of the dependence on the thermodynamic factor, *Phys. Rev.*, **E 100**, 022112 (2019).
68. Duan, J., Computer modeling of diffusion in Ni-rich Ni<sub>3</sub>Al and composition dependence of diffusion in  $\gamma$  Ni<sub>3</sub>Al, *J. Phys. Condens. Matter*, **20**, 195221 (2008).

69. Zhang, G., Fan, X., Zhang, Q., Li, Q., Li, M., Partial disordering and homogeneous melting in multicomponent systems, *Acta Mater.*, **239**, 11828 (2022).
70. Zakharov, V.V., Combined alloying of aluminum alloys with scandium and zirconium, *Metal Science and Heat Treatment*, **56**, 281 (2014).
71. Di Pietro Martínez, D., Hoyuelos, M., Diffusion in binary mixtures: An analysis of the dependence on the thermodynamic factor, *Phys. Rev., E* **100**, 022112 (2019).
72. Manning, J.R., *Diffusion Kinetics for Atoms in Crystals*, van Norstrand, Princeton, 1968; J.R. Manning, *Acta Metall.* **15**, 817 (1967)
73. Wang, W.Y., Shang, S.L., Fang, H.Z., Zhang, H., Wang, Y., Mathaudhu, S.N., Hui, Z.D., Liu, Z.-K., Effects of Composition on Atomic Structure, Diffusivity, and Viscosity of Liquid Al-Zr Alloys, *Metal. And Mater., Transactions, A*, **43**, 3471 (2012).
74. Srinivasan, D., Chattopadhyay, K., Non-equilibrium transformations involving L1 2-Al 3 Zr in ternary Al-X-Zr alloys. *Metallurgical and Materials Transactions A*, **36**, 311 (2005).